sustainability

MDPI

Article

Feasibility Limits in Corridor-Wide EV Fast-Charging Station Planning for Sustainable Transport Electrification: An MILP Study of Puerto Rico's PR-2

G. Alejandra Feo-Cediel [1,*], Daniel D. Campo-Ossa [2], Adriana C. Luna-Hernández [3], Agustín Irizarry-Rivera [1] and Fabio Andrade-Rengifo [1,*]

[1] Department of Electrical and Computer Engineering, University of Puerto Rico at Mayagüez, Mayagüez, PR 00680, USA; agustin.irizarry@upr.edu
[2] Department of Technology and Applied Sciences, University of Puerto Rico at Aguadilla, Aguadilla, PR 00604, USA; daniel.campo@upr.edu
[3] Engineering Faculty, Universidad Distrital Francisco José de Caldas, Bogotá 111711, Colombia; aclunah@udistrital.edu.co
* Correspondence: guisellealejandra.feo@upr.edu (G.A.F.-C.); fabio.andrade@upr.edu (F.A.-R.)

Abstract

Planning fast-charging infrastructure for electric vehicles (EVs) supports sustainable transport electrification. This study identifies when a corridor-wide plan along Puerto Rico Highway 2 (PR-2) becomes infeasible and which modeled constraint limits it first. A mixed-integer linear programming (MILP) model with 229 candidate sites across 27 municipalities, integer 150 kW port decisions, a 3 MW per-site ceiling, corridor coverage, and a shared upstream-capacity screen is solved for a February 2024 baseline and six electrification scenarios under an upper-bound demand assumption. The baseline is feasible with 30 stations, 178 ports, and 26.7 MW, whereas all six future scenarios are infeasible. San Juan and Guaynabo, which hold one-third of the island's registered EV stock but four candidate sites each, exhaust their candidate-set capacity first, at closed-form thresholds of 1.78% and 3.38% electrification, versus 8.99% in the calibrated-2030 case. This threshold reproduces the MILP shortfall to four decimal places in all six infeasible scenarios. At a screening fraction of 0.20, removing the upstream screen changes neither feasibility nor shortfall. Restoring 2030 feasibility would require at least 21 and 11 represented 3 MW sites, versus four each. Under the modeled assumptions, these findings support examining candidate-site limitations before upstream grid reinforcement in sustainable corridor planning.

Keywords: EV fast charging; charging-station siting; mixed-integer linear programming; feasibility diagnostic; electrification scenarios; grid-capacity screening; island power systems; sustainable transportation; Puerto Rico

Check for updates

Academic Editors: Carlos Vargas-Salgado and Jesus Aguila-Leon

Received: 4 October 2026
Revised: 21 October 2026
Accepted: 22 October 2026
Published: 25 October 2026

Copyright: © 2026 by the authors. Licensee MDPI, Basel, Switzerland. This article is an open access article distributed under the terms and conditions of the Creative Commons Attribution (CC BY) license.

1. Introduction

Electric vehicles (EVs) contribute to the transition toward sustainable, low-carbon transportation. Global electric-car sales reached nearly 14 million in 2023, about 18% of all new cars sold, and the number of installed public charging points grew by 40% in the same year [1]. In addition to eliminating tailpipe emissions, EVs can reduce reliance on imported fuels, provide environmental and public-health benefits, and support grid services through managed charging, including bidirectional vehicle-to-grid and vehicle-to-home operation [2], advantages that are particularly relevant for islands and remote power systems [3]. However, high purchase costs, limited driving range, and inadequate charging

availability continue to hinder EV adoption, making public fast-charging infrastructure important for wider uptake [4]. Fast charging also shifts part of the transportation energy demand to the electricity system: fast-charging stations create concentrated loads whose siting and sizing must account for mobility access, spatial coverage, and local grid conditions, and high EV penetration raises planning, operation, and grid-integration challenges [5,6]. These interactions are especially important in island systems, where limited generation reserves, network constraints, and resilience requirements narrow the set of practical deployment options [3,7].

Several approaches have been used to plan EV fast-charging stations (EVFCSs), each focusing on a different aspect of the problem. Geographic information system (GIS) and spatial-suitability methods identify locations where charging needs and site accessibility coincide [8,9]. Traffic-flow and probabilistic models estimate the charging energy required at individual locations [10,11]. Although useful for characterizing demand, these methods do not generally determine whether station-size and electrical constraints allow that demand to be met.

Metaheuristic methods can address nonlinear and multi-objective trade-offs among cost, losses, and service quality [12,13]. However, they generally cannot certify global optimality or infeasibility, so failing to find a feasible solution does not show that none exists. Coupled transportation–power-network and distribution-level models represent electrical constraints, losses, and hosting capacity explicitly [14–16], and island studies have combined charging deployment with alternating-current (AC) power-flow analysis, generation planning, or microgrid design [7,17–19]. These models provide greater electrical detail but require network data, such as impedances, loading, and certified hosting capacity, that are rarely available for every candidate site along a long corridor at the planning stage.

Mixed-integer linear programming (MILP) formulations jointly determine station location, discrete capacity, and demand allocation along highways and corridors [20–22]. When an exact solver terminates with the corresponding certificate, it establishes either optimality or infeasibility under the adopted formulation. Recent reviews organize the field around station placement, sizing, grid upgrades, and uncertainty [23,24].

Most of these studies ask where charging stations should be installed and how much capacity they should provide, typically assuming that a feasible deployment exists. Land-constrained, robust-siting, and hosting-capacity studies show that limiting conditions, including the availability of admissible candidate locations, can become binding [16,25,26], but they generally examine a given deployment or a single constraint class. As electrification grows, the question is no longer only where to install charging capacity, but whether the represented candidate sites can accommodate it: at what electrification level does a corridor-wide plan cease to be feasible under the adopted planning representation, which modeled constraint becomes limiting first, and can that limit be quantified before detailed grid studies are undertaken?

This diagnostic question motivates the use of MILP in this study. The formulation represents site selection and integer port counts directly. When an exact solver returns an infeasibility certificate, no plan satisfies the full-service model under the stated assumptions; the solver has not merely failed to find one. The same model can then be relaxed to locate and measure the resulting municipal shortfall. A linear screen of shared upstream-segment capacity is less detailed than AC power flow, but it can be removed and restored in otherwise identical model runs, which isolates its contribution to infeasibility.

The distinguishing element of this study is therefore the combination of a corridor-wide MILP, a municipal shortfall diagnostic, a paired upstream-capacity benchmark, and a closed-form candidate-set threshold. The approach is not proposed as generally superior

to existing methods; it addresses a specific planning question that complements them. Detailed power-flow and interconnection studies remain necessary to assess the physical feasibility of the locations it identifies.

Puerto Rico provides a relevant case for sustainable transport electrification because its high dependence on automobiles coincides with an island power system undergoing grid modernization and a transition toward renewable energy [27,28]. Current resource-adequacy proceedings also document generation-sufficiency stress, recurrent manual load shedding, and continuing emergency-generation measures [29–32]. These system-level conditions are distinct from the shared upstream-capacity screen used in this model, which makes it essential to separate what a corridor-planning screen can identify from what requires a detailed power-system study. Highway PR-2, an interregional corridor that crosses 27 municipalities including the San Juan metropolitan area, is used as the study corridor (Section 2.1). Because long-horizon EV forecasts depend strongly on model structure, assumptions, and input data, with errors that grow with the prediction horizon [33], no single adoption trajectory is treated as a deterministic forecast. The electrification pathways are instead taken from a preceding Puerto Rico study that established planning-reference envelopes, a calibrated generalized-logistic trajectory, drivetrain-definition cases, and calibration-uncertainty bounds [34]. That study did not model spatial EVFCS deployment, charging-port decisions, or grid-capacity-constrained siting. The pathways are used solely as exogenous scenario inputs; the present study applies and extends a corridor-wide EVFCS planning framework through feasibility diagnostics, an upstream-capacity benchmark, and analytical candidate-set thresholds.

Accordingly, this study investigates which modeled constraints limit the ability of the PR-2 charging-infrastructure representation to accommodate increasing EV fast-charging demand, and how charging-demand assumptions, station-capacity limits, and candidate-site availability affect municipal feasibility thresholds. The analysis focuses particularly on whether the finite charging capacity represented by municipal candidate sets becomes limiting before the shared upstream-capacity screen under the primary planning assumptions.

This study makes three contributions. First, EVFCS deployment along PR-2 is formulated as a single corridor-wide MILP with integer port counts, corridor coverage, municipal demand service, and shared upstream-segment capacity, coupled with an infeasibility diagnostic that quantifies the municipal shortfall when full service cannot be met. Second, each primary scenario is solved with and without the shared upstream-capacity constraint, and the screening fraction is varied, which isolates the contribution of that layer and assesses whether it determines the diagnostic optimum under the primary planning assumptions. Third, a closed-form candidate-set capacity threshold, P_m^{crit}, is derived as a necessary municipal feasibility condition. Under the primary assumptions and the aggregate municipal-demand representation adopted here, the shortfall implied by this threshold coincides with the MILP diagnostic shortfall to four decimal places in all six infeasible future scenarios. The effects of fast-charging demand, station-size limits, candidate-set size, municipal shares, drivetrain definition, and calibration uncertainty can therefore be quantified analytically.

2. Case Study, Data, and Planning Assumptions

2.1. Puerto Rico and the PR-2 Case Study

PR-2 was selected as the study corridor because it is a major interregional highway extending across a substantial portion of Puerto Rico and, within the adopted corridor representation, spans 27 municipalities. Under the adopted registration-based demand allocation, the 27 corridor municipalities account for 62.4% of the island's baseline electrified-vehicle stock. This concentration makes PR-2 a relevant case for evaluating corridor-planning

feasibility limits, although registered vehicle stock does not directly measure observed fast-charging activity along the highway. Municipal electrified-vehicle stock information is obtained from the Puerto Rico Department of Transportation and Public Works (DTOP) [35], while the candidate locations can be associated with nearby upstream electrical segments using the Puerto Rico Electric Infrastructure GIS [36]. Together, these data allow spatial access, charging demand, and electrical screening to be evaluated within a common corridor-wide framework. The future electrification levels considered in this study are planning pathways rather than statutory vehicle-fleet targets [34]. Puerto Rico's Energy Public Policy Act (Law 17-2019) establishes a target of 100% renewable electricity by 2050, providing a policy context for sustainable transport electrification and the associated expansion of charging infrastructure [37]. Law 33-2019 provides the broader resilience context, Law 81-2014 supports EV adoption and charging infrastructure, and the National Electric Vehicle Infrastructure (NEVI) Formula Program motivates the corridor-spacing and minimum-power screens adopted here [38–40]. In this study, a planning screen denotes a simplified preliminary feasibility assessment used to identify potentially limiting conditions before detailed engineering or interconnection studies are performed. Accordingly, the formulation should not be interpreted as either NEVI certification or a utility interconnection study.

2.2. Data Sources and GIS Preprocessing

Candidate sites were generated at approximately 1 km intervals along PR-2 using OpenStreetMap coordinates processed in QGIS. This interval defines the spatial resolution of the model rather than a physical siting requirement; it samples the corridor densely relative to the 80.5 km maximum-spacing screen and yields 229 candidate locations. These candidates are modeled corridor locations, not parcels verified for physical, commercial, or legal EVFCS deployment: land use, zoning, right-of-way restrictions, and parcel availability were not assessed. Because candidates are distributed uniformly along the highway, municipalities with shorter PR-2 segments have fewer represented sites, regardless of their registered vehicle stock. This property becomes central in Section 4.3: San Juan and Guaynabo hold substantial shares of the registered electrified-vehicle stock but only four candidate locations each. The candidate set was linked to transmission-infrastructure layers from the Puerto Rico Electric Infrastructure GIS repository [36]. For each site u, preprocessing retains up to three alternatives corresponding to the nearest available 38, 115, and 230 kV transmission segments. These segments serve only as references for upstream-capacity screening and are not assumed to represent station service voltages, physical points of interconnection, or verified distribution-level hosting capacity. Figure 1 illustrates the resulting spatial association between PR-2 candidate sites and the upstream electrical layers used in the screening model.

Each transmission segment is identified by a GIS feature identifier (FID). Let E denote the set of unique upstream segments and $E_u \subseteq E$ the alternatives available to site u. Because multiple candidates can map to the same segment, screened capacity is enforced once at the segment level rather than independently at each site. Conductor ampacity and resistance parameters are derived from GIS attributes and manufacturer documentation from Southwire and Brugg Cables [41,42]. One 38 kV FID was associated with two candidates more than 200 km apart and with different conductor ratings (15.1 and 48.0 MVA); these records were disambiguated using the tuple (voltage, FID, rating). No other collision was identified among the 494 voltage–segment combinations.

Municipal demand inputs are based on DTOP registration data [35]. The analysis is limited to light-duty electrified vehicle lines; medium- and heavy-duty electrification is outside the present scope and is addressed separately in the Puerto Rico Grid Resilience and Transitions to 100% Renewable Energy Study (PR100) [43]. Because the registration series is broader than a battery electric vehicle (BEV)-only fleet, the resulting fast-charging demand

is treated as an upper-bound planning screen [34]. The February 2024 baseline contains 17,784 registered vehicles and was reported as a descriptive observation in the preceding study, but was not used in its 2014–2023 diffusion-model calibration [34]. This February 2024 dataset is retained as the observed-stock baseline because it is the available municipal source that identifies electrified model lines, which the demand allocation requires. An official municipality-level report of vehicles with active registration (*marbete activo*) as of 30 June 2026 [44] is a general registration summary rather than an electrified-vehicle record: it aggregates vehicles by category (automobile, truck, motorcycle, bus, and trailer) rather than by drivetrain. Its totals are therefore not comparable with the electrified-vehicle baseline and cannot be used to update the municipal allocation shares without drivetrain-specific records. The baseline is accordingly an observed reference cross-section, not a claim that the municipal stock remained unchanged after February 2024. Narrower drivetrain definitions are evaluated analytically against the candidate-set feasibility threshold in Section 4.3 rather than rerun through the full MILP.

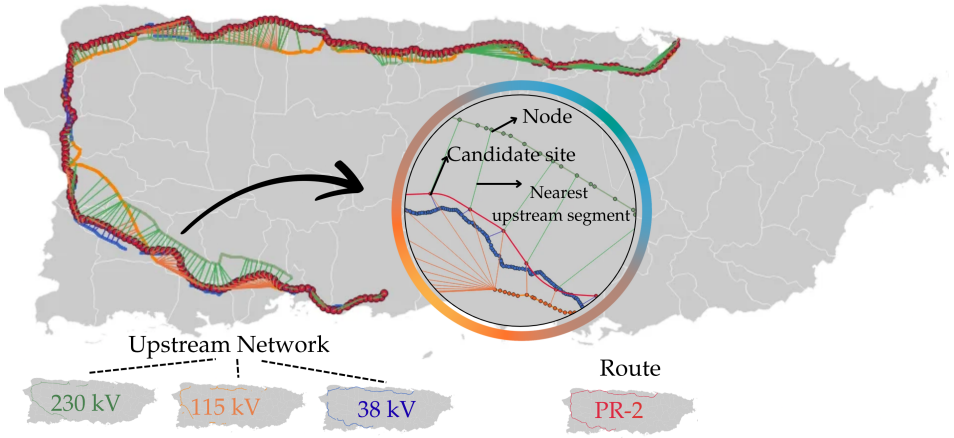


Figure 1. Geographic information system (GIS) preprocessing used to associate Puerto Rico Highway 2 (PR-2) candidate sites with nearby upstream electrical segments at 38, 115, and 230 kV. For each candidate, the nearest available segment at each represented voltage level is retained as a planning-screening alternative.

The links between data sources and model inputs are summarized in Table 1.

Table 1. Data sources and their roles in the corridor-wide planning model.

Data	Source	Resolution	Use in the Model
Electrified-vehicle registrations	DTOP [35]	Municipality	Baseline stock $N_{m,0}$ and municipal allocation shares s_m
EV diffusion parameters	Feo-Cediel et al. [34]	Island-wide annual series	Published calibrated stock $S_{EV}(t)$, drivetrain-definition cases, and calibration-uncertainty bounds
PR-2 geometry	OpenStreetMap	1 km corridor discretization	Candidate set U, service checkpoints J, and longitudinal coordinates
Transmission GIS	Puerto Rico Electric Infrastructure GIS [36]	Electrical segment/FID	Upstream resource set E, alternatives E_u, voltage layer, and connection distance
Conductor data	GIS attributes and manufacturer documentation [41,42]	Electrical segment	Segment thermal rating S_e, connection-resistance parameters, and screened capacity $C_e(\phi_e)$

DTOP, Puerto Rico Department of Transportation and Public Works; EV, electric vehicle; FID, feature identifier.

2.3. Planning Assumptions

Table 2 distinguishes fixed planning assumptions from parameters examined analytically or through sensitivity analysis. Two assumptions have opposing implications for feasibility and should be considered together. The fast-charging fraction $f_{FC} = 1$ assigns one representative fast-charging event per modeled vehicle per day and therefore sets an upper bound on modeled fast-charging demand; it is a planning screen rather than an estimate of observed charging behavior. The utilization factor $\eta_{use} = 1$ assumes that installed capacity is available throughout the 24 h planning window, which is the most favorable value for energy delivery. The primary case thus combines an upper-bound demand assignment with an idealized supply-side assumption. Because infeasibility at $\eta_{use} = 1$ implies infeasibility at any lower utilization, the identified limits do not rest on an optimistic utilization assumption, whereas their magnitude does depend on the demand assignment. Both parameters, along with the station-size ceiling x^{max} and the candidate-set size $|U_m|$, are therefore evaluated separately in Section 4.5.

Table 2. Principal planning assumptions used in the baseline and robustness analyses.

Quantity	Baseline Value	Treatment	Interpretation
Port power P^{ch}	150 kW	Fixed	Representative direct-current (DC) fast-charging port rating
Charging-event duration t_s	0.25 h	Fixed	Representative 15 min planning event
Ports per selected station	4–20	Baseline bound; tested analytically through x^{max}	600–3000 kW station range in the primary MILP
Fast-charging demand fraction f_{FC}	1.00	Bounded analytically	Fraction of the modeled stock assigned one representative fast-charging event per day; $f_{FC} = 1$ defines the upper-bound demand screen
Power factor pf	1	Fixed screening assumption	Converts segment apparent-power rating to a numerically equivalent active-power screen
Upstream-capacity screening fraction ϕ	0.20	Swept, $\phi \in [0.005, 0.20]$	Fraction of estimated nominal thermal rating used for EVFCS planning-screen purposes
Effective utilization η_{use}	1.00	Bounded analytically (Equation (29))	Fraction of the 24 h planning window effectively available at installed power; $\eta_{use} = 1$ is the most favorable case, so infeasibility at $\eta_{use} = 1$ implies infeasibility for all $\eta_{use} < 1$
Maximum spacing d^{max}	80.5 km	Fixed planning screen	NEVI-inspired 50-mile corridor-spacing requirement
Municipal minimum	One EVFCS per corridor municipality	Constraint-removal test (baseline case)	Equity/access planning requirement distinct from corridor coverage

EVFCS, electric vehicle fast-charging station; MILP, mixed-integer linear programming; NEVI, National Electric Vehicle Infrastructure.

The per-site ceiling $x^{max} = 3$ MW is defined by the adopted station-sizing configuration of up to $n^{max} = 20$ DC fast-charging ports, each rated at $P^{ch} = 150$ kW. Accordingly, $x^{max} = n^{max} P^{ch} = 20 \times 150$ kW $= 3$ MW. A 20-charger station size has been reported in charging-infrastructure planning literature [24], and 150 kW is a documented DC fast-charging power

level [6]. A utility-oriented highway planning example also considers an illustrative service-plaza configuration of 20 × 150 kW = 3 MW [45]. The maximum of 20 ports is an adopted planning assumption, not a requirement of the NEVI program. Therefore, the 3 MW ceiling is neither a regulatory maximum nor a utility-certified interconnection limit. Sensitivity cases considering $x^{\max} > 3$ MW represent hypothetical relaxations of the 20-port constraint or changes in the charging configuration; they are not directly implementable within the primary formulation. The effects of station capacity and candidate-site availability on the municipal feasibility thresholds are evaluated in Section 4.5.

3. Corridor-Wide EVFCS Planning Methodology

The methodology consists of five steps. Published electrification pathways are first converted into municipal charging-energy demand. The resulting demands are combined with PR-2 candidate locations and GIS-identified upstream segments in a single corridor-wide MILP. The full-service model is the original MILP in which all modeled municipal charging demand must be satisfied without demand-shortfall variables. When that model is infeasible, a separate municipal shortfall diagnostic identifies the location and magnitude of the demand–capacity mismatch. A closed-form candidate-set threshold is then used to characterize how municipal feasibility depends on demand assignment, candidate-set size, station-size limits, utilization, and municipal allocation. Finally, paired with/without-upstream-capacity-screen tests and a sensitivity sweep in ϕ determine whether the shared upstream-capacity constraint changes the limiting condition.

3.1. EV Adoption and Municipal Charging Demand

The calibrated future-electrification case is imported, without recalibration, from the previously published generalized-logistic trajectory for Puerto Rico [34]. Consistent with the notation of that study, the island-wide registered electrified-vehicle stock is denoted by $S_{\mathrm{EV}}(t)$:

$$S_{\mathrm{EV}}(t) = \frac{EV_{\max}}{[1 + \exp(-\alpha(t - t_0))]^k}, \tag{1}$$

where $EV_{\max}$ = 1,985,222 vehicles is the DTOP reference fleet, $t_0 = 2014$, $\alpha = 0.10935138$, and $k = 15.02970448$. The reference fleet is used as a planning-level normalization and upper bound rather than as a direct forecast of future fleet size. The published calibration corresponds to reference-fleet electrification levels of approximately 9.0% in 2030 and 74.8% in 2050 [34]; no diffusion-model parameters are re-estimated in the present study. The calibrated trajectory is compared with the planning-reference envelopes in Section 3.5.

Island-wide stocks are allocated to municipalities according to each municipality's share of the baseline registered stock:

$$s_m = \frac{N_{m,0}}{N_{\mathrm{island},0}}, \qquad N_m(t) = s_m S_{\mathrm{EV}}(t), \tag{2}$$

where $N_{m,0}$ and $N_{\mathrm{island},0}$ are the baseline registered stocks of municipality m and of Puerto Rico, respectively. The 27 corridor municipalities account for 11,096 of the 17,784 registered vehicles in the baseline cross-section, giving $\sum_{m \in M} s_m \approx 0.624$. The same baseline shares are applied to future island-wide stocks, including those derived from the reference fleet $EV_{\max}$. The resulting municipal stocks are therefore planning quantities rather than observed future vehicle counts. This allocation assumes that the relative geographic distribution of the registered electrified-vehicle stock remains unchanged over the planning horizon.

The energy of a representative fast-charging event is

$$E_s = P^{ch} t_s = 150\ \text{kW} \times 0.25\ \text{h} = 37.5\ \text{kWh}. \quad (3)$$

A dimensionless demand-assignment factor $f_{FC} \in (0, 1]$ is introduced to separate the energy of one representative event from the fraction of the modeled vehicle stock assigned one such event per day. The municipal charging-energy demand at time t is therefore

$$D_m(t) = f_{FC} E_s N_m(t). \quad (4)$$

In each planning scenario, $D_m(t)$ is evaluated at the corresponding scenario year and treated as the municipal demand input to the MILP. The primary analysis uses $f_{FC} = 1$, corresponding to one representative 37.5 kWh fast-charging event per modeled vehicle per day. This defines an upper-bound corridor-demand scenario rather than an estimate of observed daily charging behavior; lower values of f_{FC} are examined analytically in Section 4.5.

3.2. Candidate Sites and Upstream Grid Resources

For each upstream electrical segment $e \in E$, the nominal three-phase apparent-power rating is estimated from the conductor ampacity and nominal line-to-line voltage:

$$S_e = \sqrt{3}\, V_{LL,e}\, I_e. \quad (5)$$

At the planning-screen level, a unity power factor is assumed, pf = 1. The screened active-power capacity used for EVFCS planning is therefore represented as

$$C_e(\phi_e) = \phi_e\, \text{pf}\, S_e, \quad (6)$$

The parameter $\phi_e \in (0, 1]$ represents the fraction of the estimated nominal thermal rating of upstream segment e made available to the modeled EVFCS load for planning-screen purposes. The formulation permits segment-specific values of ϕ_e. In the primary case, however, a uniform value $\phi_e = \phi_0 = 0.20$ is applied to all 38, 115, and 230 kV segments because utility-certified segment- or voltage-specific available-capacity margins are unavailable for the candidate set considered here. Using a common value avoids introducing unsupported voltage-specific precision while retaining the ability to apply differentiated values when certified margins become available. Accordingly, $\phi_0 = 0.20$ is treated as a planning-screening assumption, and its influence is evaluated explicitly in Section 4.6.

Because pf and ϕ_e enter Equation (6) multiplicatively, a non-unity power factor is equivalent within this thermal-capacity screen to a proportional reduction in the effective screening fraction, $\phi_{\text{eff}} = \phi_e\, \text{pf}$. The ϕ-sensitivity analysis therefore also captures the corresponding effect of moderate departures from unity power factor. For example, $\phi = 0.20$ with pf = 0.95 gives $\phi_{\text{eff}} = 0.19$, which lies within the range over which the benchmark result remains unchanged.

Connection distance affects only the secondary ranking criterion of the lexicographic objective. The GIS preprocessing provides the distance between each candidate site u and upstream segment e. Let d_{ue}^{conn} denote this distance and r_{ue}^{conn} the representative resistance per unit length of the assumed connection conductor. The corresponding connection resistance is

$$R_{ue} = r_{ue}^{\text{conn}} d_{ue}^{\text{conn}}. \quad (7)$$

Using the primary maximum station capacity $x^{\max} = 3000$ kW, a common reference current is calculated for each voltage layer:

$$I_e^{\text{ref}} = \frac{x^{\max}}{\sqrt{3}\, V_{LL,e}\, \text{pf}}. \quad (8)$$

The corresponding reference full-load connection-loss proxy is

$$\overline{P}_{ue}^{\text{loss}} = 3\left(I_e^{\text{ref}}\right)^2 R_{ue}. \tag{9}$$

$\overline{P}_{ue}^{\text{loss}}$ is evaluated at the common reference capacity $x^{\max} = 3$ MW and is therefore a full-load connection-ranking quantity rather than the operating loss of a particular station. To account for assigned-capacity differences without sacrificing linearity, the secondary objective scales this reference quantity by $x_{ue}/x^{\max}$. The resulting capacity-weighted proxy equals $\overline{P}_{ue}^{\text{loss}}$ at $x_{ue} = x^{\max}$ and decreases proportionally for smaller assignments.

3.3. MILP Formulation

In plain terms, the model can be summarized as follows. Each of the 229 candidate locations either hosts a station or does not; a selected station receives a whole number of 150 kW ports, up to the 3 MW ceiling. Each municipality must receive, within its own candidates, enough installed charging capacity to serve its daily charging-energy demand, and each corridor municipality hosts at least one station. Stations must be spaced so that no stretch of PR-2 exceeds the maximum-spacing criterion, and each station is connected to one nearby upstream electrical segment whose screened capacity is shared by all stations connected to it. Among all plans that satisfy these rules, the model selects the one with the least total installed capacity and, among those, the one with the smallest connection-loss proxy. If no plan satisfies all rules, the full-service model is infeasible, and the diagnostic in Section 3.4 measures how much demand cannot be served and where.

The EVFCS planning problem is formulated as a single corridor-wide MILP. Each candidate site belongs to one municipality, whereas an upstream electrical segment may be shared by candidate sites in different municipalities. This distinction allows local demand requirements to be represented together with shared electrical-resource limits. Table 3 summarizes the sets, parameters, and decision variables. Figure 2 illustrates this structure. Candidate sites u are grouped by municipality m, each with charging-energy requirement D_m. A selected site ($y_u = 1$) contains an integer number of charging ports n_u and has installed capacity $x_u = P^{\text{ch}} n_u$. Each selected site is assigned through z_{ue} to exactly one available upstream segment $e \in E_u$, and its capacity x_{ue} is attributed to that segment. Because sites in different municipalities may use the same segment, they share its screened capacity $C_e(\phi_e)$ through Equation (18). The interlaced 38, 115, and 230 kV traces in the figure represent only the changing geographic proximity of the upstream voltage layers along PR-2; they do not imply electrical interconnection between the displayed segments.

Table 3. Sets, parameters, and decision variables used in the corridor-wide MILP.

Symbol	Description
Sets	
U	Candidate EVFCS sites along PR-2
M	Municipalities intersected by the PR-2 corridor
U_m	Candidate sites located in municipality m
E	Unique upstream electrical segments identified by GIS FID
E_u	Upstream electrical alternatives available to site u
J	Corridor service checkpoints used for the spacing screen
Parameters	
D_m	Daily planning-screen charging-energy demand in municipality m (kWh/day)

Table 3. *Cont.*

Symbol	Description
P^{ch}	Rated power of one fast-charging port (kW)
E_{s}	Energy of one representative fast-charging event (kWh)
f_{FC}	Fraction of the modeled stock assigned one representative fast-charging event per day
$n^{\min}, n^{\max}$	Minimum and maximum ports per selected station
$x^{\max}$	Maximum installed capacity of one station (kW)
S_e	Nominal apparent-power rating of upstream segment e (kVA)
$V_{LL,e}$	Nominal line-to-line voltage of upstream segment e (kV)
I_e	Conductor ampacity associated with upstream segment e (A)
$C_e(\phi_e)$	Screened active-power capacity of upstream segment e used for EVFCS planning (kW)
pf	Power factor used in the upstream-capacity and reference-current calculations
ϕ_e	Upstream-capacity screening fraction for segment e; ϕ denotes the uniform value used in the primary and sensitivity cases, with $\phi_e = \phi, \forall e \in E$
d_{ue}^{conn}	Distance between candidate site u and upstream segment e (km)
r_{ue}^{conn}	Representative connection-conductor resistance per unit length (Ω/km)
R_{ue}	Representative connection resistance for site–segment pair (u, e) (Ω)
$\overline{P}_{ue}^{\mathrm{loss}}$	Reference full-load connection-loss proxy for site u and segment e (kW)
d_u, d_j	Longitudinal PR-2 coordinates of candidate u and checkpoint j (km)
R^{cov}	Corridor service radius used in the set-covering constraint (km)
η_{use}	Effective utilization factor within the 24 h planning window
τ_{use}	Effective utilization time, $24\eta_{\mathrm{use}}$ (h/day)
Decision variables	
y_u	Binary variable equal to 1 if an EVFCS is installed at site u
n_u	Integer number of fast-charging ports installed at site u
x_u	Installed charging capacity at site u (kW)
z_{ue}	Binary variable equal to 1 if site u uses upstream segment e
x_{ue}	Capacity assigned from upstream segment e to site u (kW)

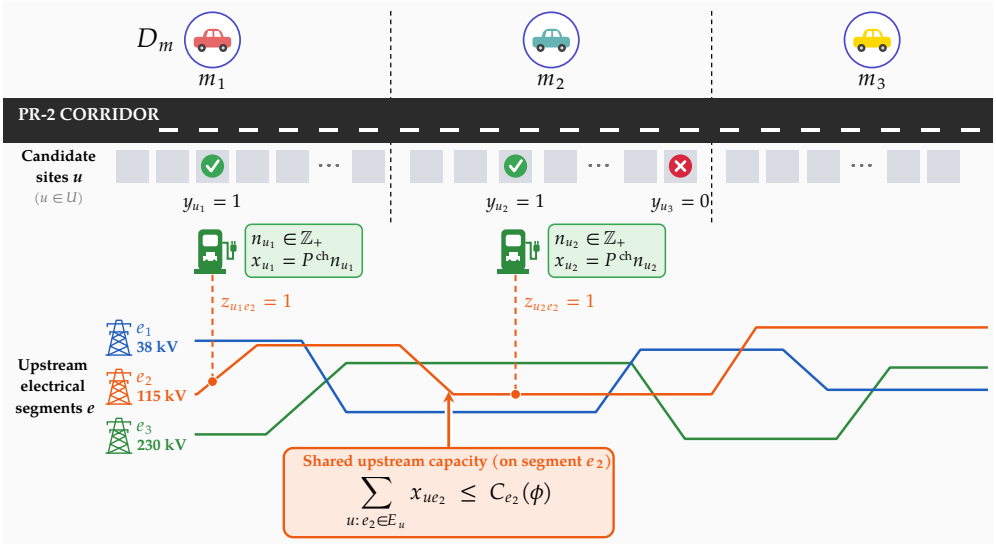


Figure 2. Schematic of the corridor-wide MILP: candidate sites grouped by municipality, integer port decisions, and assignment of each selected site to one shared upstream segment.

3.3.1. Lexicographic Objective

The lexicographic objective prioritizes minimizing installed charging capacity over minimizing the connection-loss proxy [46]. Here, $\mathcal{F}$ denotes the set of all decision-variable combinations satisfying the constraints defined below. In the first stage, total installed capacity is minimized over $\mathcal{F}$:

$$X^\star = \min_{(x,y,n,z,x_{ue})\in\mathcal{F}} \sum_{u\in U} x_u. \tag{10}$$

After the optimum $X^\star$ is obtained, the second stage minimizes a linear capacity-weighted connection proxy among capacity-optimal solutions:

$$\min_{(x,y,n,z,x_{ue})\in\mathcal{F}} \sum_{u\in U}\sum_{e\in E_u} \frac{\overline{P}^{\text{loss}}_{ue}}{x^{\max}} x_{ue}, \tag{11}$$

subject to

$$\sum_{u\in U} x_u = X^\star. \tag{12}$$

Because $\sum_{u\in U} x_u = X^\star$ is fixed in the second stage, the objective of Equation (11) can only distinguish among capacity-optimal solutions. Because the coefficient $\overline{P}^{\text{loss}}_{ue}/x^{\max}$ multiplies the capacity x_{ue} actually assigned to connection (u,e), the ranking scales with assigned capacity instead of treating every connection as if it carried the full $x^{\max}$ reference load. This lexicographic formulation avoids an arbitrary weighting coefficient between the two objectives. An audit-only variant of Equation (11) that reproduces the original fixed full-load ranking, $\sum_{u,e} \overline{P}^{\text{loss}}_{ue} z_{ue}$, is retained in the implementation to verify that this refinement does not alter the primary capacity results (Section 4.1).

3.3.2. Station Size and Integer Port Count

A selected station must contain between $n^{\min} = 4$ and $n^{\max} = 20$ fast-charging ports:

$$n^{\min} y_u \le n_u \le n^{\max} y_u, \qquad \forall u \in U, \tag{13}$$

with

$$x_u = P^{\text{ch}} n_u, \qquad \forall u \in U. \tag{14}$$

For $P^{\text{ch}} = 150$ kW, the selected-station range is 600–3000 kW.

3.3.3. Upstream-Segment Selection and Capacity Assignment

Each selected site uses exactly one of its available upstream electrical alternatives:

$$\sum_{e\in E_u} z_{ue} = y_u, \qquad \forall u \in U. \tag{15}$$

The station capacity is assigned to the selected segment through

$$x_u = \sum_{e\in E_u} x_{ue}, \qquad \forall u \in U, \tag{16}$$

and

$$0 \le x_{ue} \le x^{\max} z_{ue}, \qquad \forall u \in U,\ \forall e \in E_u. \tag{17}$$

Equation (17) uses the physical station upper bound $x^{\max} = 3000$ kW directly, avoiding the need for a separate generic Big-M constant.

3.3.4. Shared Upstream-Capacity Constraint

The upstream-capacity constraint represents a planning-level limit on the amount of EVFCS capacity that can be assigned to a shared upstream electrical segment. It uses a screened fraction of the segment's estimated thermal rating and does not represent generation adequacy, substation capacity, detailed distribution-network hosting capacity, or full power-flow feasibility. If several candidate sites map to the same upstream electrical segment, their assigned capacities share the same screened resource:

$$\sum_{\substack{u \in U: \\ e \in E_u}} x_{ue} \le C_e(\phi_e), \qquad \forall e \in E. \tag{18}$$

The segment-level constraint prevents the same screened upstream capacity from being counted independently for multiple candidate sites.

3.3.5. Municipal Demand

The aggregate deliverable charging energy assigned to municipality m must meet its planning-screen demand:

$$\sum_{u \in U_m} \tau_{\text{use}} x_u \ge D_m, \qquad \forall m \in M, \tag{19}$$

where

$$\tau_{\text{use}} = 24\eta_{\text{use}}, \qquad 0 < \eta_{\text{use}} \le 1. \tag{20}$$

The primary analysis uses $\eta_{\text{use}} = 1$, which is the most favorable value for feasibility. Because x_u already represents the aggregate power of all ports installed at site u, no additional multiplier for ports or charging sessions is applied in Equation (19).

A separate municipal-access condition requires at least one EVFCS in each corridor municipality:

$$\sum_{u \in U_m} y_u \ge 1, \qquad \forall m \in M. \tag{21}$$

In the full-service model, this requirement is redundant whenever $D_m > 0$, because satisfying Equation (19) already requires positive installed capacity in municipality m. It is nevertheless retained to keep the access requirement explicit and is examined through a baseline constraint-removal test. In the diagnostic relaxation, the condition remains necessary because ξ_m could otherwise absorb all municipal demand without forcing selection of a station.

3.3.6. Corridor-Wide Set-Covering Constraint

Let

$$U(j) = \left\{ u \in U : \left| d_u - d_j \right| \le R^{\text{cov}} \right\}. \tag{22}$$

be the set of candidate stations capable of serving checkpoint j. The corridor-wide coverage requirement is

$$\sum_{u \in U(j)} y_u \ge 1, \qquad \forall j \in J. \tag{23}$$

For the NEVI-inspired 50-mile maximum-spacing screen, $d^{\max} = 80.5$ km and $R^{\text{cov}} = d^{\max}/2 = 40.25$ km. Because candidate sites and service checkpoints use the same 1 km PR-2 discretization, Equation (23) applies the spacing screen on a common longitudinal grid, avoiding an additional mismatch between candidate and coverage resolutions.

The decision-variable domains are

$$x_u \ge 0, \qquad x_{ue} \ge 0, \qquad y_u \in \{0,1\}, \qquad z_{ue} \in \{0,1\}, \qquad n_u \in \mathbb{Z}_+. \tag{24}$$

3.4. Infeasibility Diagnostic and Candidate-Set Threshold

A scenario is classified as infeasible when no combination of the modeled candidate sites, station sizes, upstream assignments, and coverage decisions can simultaneously satisfy all constraints of the full-service formulation. Thus, infeasibility refers to the adopted planning representation, not necessarily to physical deployment. The full-service model enforces Equation (19) without slack. When that model is infeasible, a separate diagnostic relaxation is solved to identify the municipalities in which the modeled demand exceeds the capacity that can be assigned under the remaining constraints. A nonnegative municipal shortfall variable ξ_m is introduced only in this diagnostic model:

$$\sum_{u \in U_m} \tau_{\text{use}} x_u + \xi_m \geq D_m, \qquad \xi_m \geq 0, \qquad \forall m \in M. \tag{25}$$

The diagnostic minimizes the aggregate normalized municipal shortfall, denoted by $\Delta^\star$:

$$\Delta^\star = \min \sum_{m \in M} \frac{\xi_m}{D_m}. \tag{26}$$

No secondary capacity or loss objective is imposed in the diagnostic problem. Because $\Delta^\star$ sums municipality-level relative shortfalls, it can exceed 1. To provide a corridor-wide energy interpretation, the corridor-wide unmet-energy fraction, denoted by $\rho^\star$, is

$$\rho^\star = \frac{\sum_{m \in M} \xi_m}{\sum_{m \in M} D_m}, \qquad 0 \leq \rho^\star \leq 1. \tag{27}$$

A municipality with $\xi_m > 0$ belongs to the diagnostic shortfall set, and $\rho^\star$ reports the fraction of total modeled corridor demand that remains unmet in the relaxed solution.

To attribute the diagnostic shortfall analytically, a necessary condition for municipal feasibility is derived that can be evaluated without solving the MILP. The maximum charging capacity represented by the candidate set in municipality m is

$$\overline{X}_m = |U_m| x^{\max}. \tag{28}$$

In words, $\overline{X}_m$ is the largest charging capacity the model is allowed to place in municipality m: the number of represented candidate sites multiplied by the per-site ceiling; it is a property of the adopted representation, not a physical municipal capacity limit. Using $D_m = f_{\text{FC}} E_s s_m \big(P(t)/100\big) EV_{\max}$, the requirement $\tau_{\text{use}} \overline{X}_m \geq D_m$ gives the candidate-set capacity threshold

$$P_m^{\text{crit}} = \frac{100 \times 24\, \eta_{\text{use}}\, |U_m|\, x^{\max}}{f_{\text{FC}} E_s\, s_m\, EV_{\max}}. \tag{29}$$

Thus, P_m^{crit} represents the reference-fleet electrification percentage at which the charging capacity represented by municipality m's adopted candidate set is exhausted under the stated assumptions. It scales linearly with η_{use}, $|U_m|$, and $x^{\max}$, and inversely with f_{FC} and s_m; consequently, demand-side feasibility depends on the ratio $\eta_{\text{use}}/f_{\text{FC}}$.

The same ceiling yields the municipality-level diagnostic shortfall ratio

$$r_m(P) = \max\left(0,\, 1 - \frac{P_m^{\text{crit}}}{P}\right). \tag{30}$$

Because the municipal demand balance in Equation (19), on which $\overline{X}_m$ in Equation (28) and P_m^{crit} are based, does not resolve the spatial distribution of demand within a municipality, the threshold is a necessary but not generally sufficient condition for full MILP feasibility; corridor coverage and shared upstream-capacity constraints may also become binding.

Because Equation (29) is closed-form, it also yields the analytical sensitivity relations used in Section 4. Let $P_{m,0}^{\text{crit}}$ denote the threshold evaluated at the primary values $f_{\text{FC}} = 1$,

$\eta_{\text{use}} = 1$, $x_0^{\max} = 3$ MW, and the original candidate set. For a target electrification level P, candidate-set feasibility requires a fast-charging fraction

$$f_{\text{FC}} \leq \eta_{\text{use}} \frac{P_{m,0}^{\text{crit}}}{P}, \tag{31}$$

or, holding the other parameters at their primary values, a per-site ceiling

$$x_{m,\text{req}}^{\max} = x_0^{\max} \frac{P}{P_{m,0}^{\text{crit}}}, \tag{32}$$

or a candidate-set multiplier q_U, with $|U_m|' = q_U |U_m|$, such that

$$P_m^{\text{crit}\prime} = q_U P_{m,0}^{\text{crit}}, \qquad q_U \geq \frac{P}{P_{m,0}^{\text{crit}}} \tag{33}$$

Similarly, a perturbed municipal share $s_m' = q_m s_m$ changes the threshold to $P_m^{\text{crit}\prime} = P_m^{\text{crit}}/q_m$, so that candidate-set feasibility at level P requires

$$q_m \leq \frac{P_m^{\text{crit}}}{P}. \tag{34}$$

These relations isolate the candidate-set effect only; they do not certify feasibility of the complete MILP after the corresponding bounds are changed.

3.5. Scenario and Benchmark Design

The corridor-wide model is evaluated for a February 2024 observed-stock baseline and six future electrification cases imported, without recalibration, from the preceding Puerto Rico consistency-assessment study [34]. The future set comprises the published calibrated generalized-logistic trajectory of Equation (1) for 2030 and 2050, the three published planning-reference envelopes for 2030, and their common 100% planning-reference endpoint in 2050. The envelopes are defined by

$$P_p(t) = 100\left(\frac{t - t_0}{2050 - t_0}\right)^p, \qquad t_0 = 2014, \tag{35}$$

where $P_p(t)$ is the reference-fleet electrification level in percent and $p \in \{0.5, 1, 2\}$ defines the front-loaded (Envelope A), linear (Envelope B), and delayed (Envelope C) pathways, respectively [34]. Because all three envelopes satisfy $P_p(2050) = 100\%$, their 2050 endpoint is evaluated only once.

The seven primary scenarios are listed in Table 4.

Figure 3 shows the electrification pathways corresponding to these scenarios. For each planning-reference envelope, the corresponding island-wide stock is $S_{\text{EV}}(t) = \big(P_p(t)/100\big)EV_{\max}$, after which the same municipal allocation shares s_m are applied. The 100% fleet endpoint is used only as a planning stress case and is distinct from the 100% renewable-electricity requirement of Law 17-2019 [34,37].

Table 4. Primary scenarios evaluated with the corridor-wide MILP. All future cases use the same 27-municipality allocation shares s_m defined in Equation (2).

Scenario	Year	Level	Basis
Observed-stock baseline	Feb. 2024	—	Registered stock in electrified model lines
Calibrated diffusion	2030	9.0%	Published generalized-logistic trajectory

Table 4. *Cont.*

Scenario	Year	Level	Basis
Envelope C (delayed, $p = 2$)	2030	19.8%	Published planning-reference envelope
Envelope B (linear, $p = 1$)	2030	44.4%	Published planning-reference envelope
Envelope A (front-loaded, $p = 0.5$)	2030	66.7%	Published planning-reference envelope
Calibrated diffusion	2050	74.8%	Published generalized-logistic trajectory
Planning-reference endpoint (A/B/C converge)	2050	100%	Shared planning-reference envelope endpoint

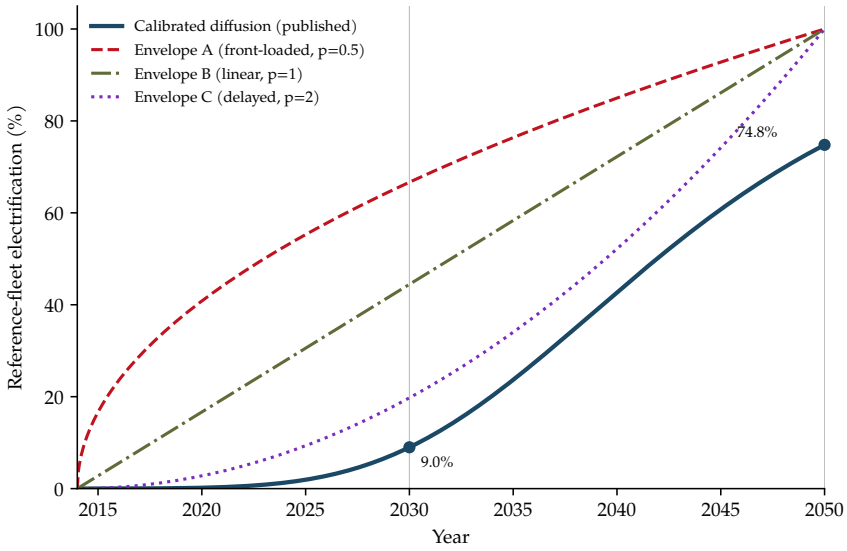


Figure 3. Reference-fleet electrification pathways used as MILP inputs: the published calibrated generalized-logistic trajectory and the three planning-reference envelopes (front-loaded, linear, and delayed), all imported from the preceding study [34].

The upstream-capacity benchmark is designed to separate candidate-set limitations from the effect of the shared upstream-capacity screen. Every scenario in Table 4 is therefore solved twice: once with Equation (18) active at $\phi_0 = 0.20$, and once with that constraint removed while demand, port bounds, municipal access, corridor coverage, and all other model elements remain unchanged. Differences between the paired solutions can thus be attributed specifically to the shared upstream-capacity screen.

Two supporting tests are added. First, the calibrated-2030 case is solved for $\phi \in \{0.20, 0.10, 0.05, 0.02, 0.01, 0.005\}$ to determine whether the benchmark conclusion depends on the primary value $\phi_0 = 0.20$. Second, the baseline is solved after removing the municipal-access condition in Equation (21), while retaining all other constraints, to verify whether that requirement independently affects the baseline solution.

3.6. Implementation and Verification

The MILP is implemented in Python 3.11 using the OR-Tools linear-solver interface `pywraplp` with the COIN-OR Branch and Cut (CBC) solver. Each planning scenario is solved as a single corridor-wide optimization problem rather than as 27 independent municipal

problems. For a feasible full-service case, the first solve minimizes total installed charging capacity. The resulting optimum $X^\star$ is then fixed, and a second solve minimizes the capacity-weighted connection proxy of Equation (11). When the full-service formulation is infeasible, a separate diagnostic model with municipal shortfall variables is solved instead. For the calibrated-2030 case, this diagnostic is additionally cross-checked against the lexicographic minimax variant described in Section 4.7.

Solver termination status is recorded for each run. A run that reaches the configured 60-second time limit with a feasible incumbent (CBC status `FEASIBLE`) retains that incumbent and flags it as not optimality-certified. Certified infeasibility is distinguished from termination without an optimality certificate, and time-limited cases with feasible incumbents are reported only as best-found solutions.

GIS preprocessing supplies the municipality associated with each candidate, the available upstream-segment FIDs, the segment ratings used to construct $C_e(\phi_e)$, and the site–segment connection distances used to construct $\overline{P}_{ue}^{\text{loss}}$. The reference implementation accepts an optional per-segment override ϕ_e; the primary experiments use the uniform default $\phi_e = \phi_0$, $\forall e \in E$.

Implementation verification includes constraint perturbations, forced-site cases, comparison with a non-optimized spatial allocation, and a separate per-municipality implementation check for the baseline. In this check, municipality-level outputs are computed through a separate implementation path, and their aggregate station count and installed capacity are compared with the corresponding corridor-wide results. These checks assess implementation consistency rather than external station or power-system performance. Selected sites are exported to QGIS and Folium, a Python web-mapping library, for geospatial inspection. The complete computational procedure used for scenario evaluation, feasibility diagnosis, and robustness testing is provided as Algorithm A1 in Appendix A.

Model development statement. The preceding study [34] evaluates the consistency between policy-oriented vehicle-electrification pathways and observed EV diffusion in Puerto Rico using reference adoption envelopes and a calibrated generalized-logistic trajectory, including uncertainty in adoption levels and transition timing. The resulting electrification pathways, together with the associated drivetrain-definition and calibration-uncertainty cases, are used here solely as exogenous scenario inputs. The preceding study does not provide the PR-2 charging-infrastructure optimization formulation or the feasibility diagnostics presented here. As outlined in the Introduction, the present article applies and extends a corridor-wide MILP planning framework to investigate infrastructure feasibility limits under these scenarios. Neither the underlying corridor representation nor general optimization techniques are claimed as individually novel.

4. Results

4.1. Baseline Corridor Solution

The February 2024 observed-stock baseline is feasible with 30 EVFCSs, 178 ports, and 26.7 MW of installed charging capacity. All 27 corridor municipalities are served, and no upstream segment reaches its screened capacity limit at $\phi_0 = 0.20$. The separate per-municipality implementation check described in Section 3.6 reproduces the same aggregate station count and total installed capacity, providing a consistency cross-check for the baseline implementation.

The capacity-weighted secondary objective in Equation (11) was compared with an audit-only implementation of the original fixed full-load ranking. Both formulations return the same first-stage capacity, 30 EVFCSs, 178 ports, the same 30 selected sites, and the same 30 upstream-segment assignments. They differ only in the distribution of ports between two already-selected San Juan sites. Under the fixed full-load ranking, interchanging the

17- and 4-port allocations between these two sites leaves the ranking objective unchanged, confirming the presence of tied port-allocation solutions. The capacity-weighted objective removes this indeterminacy by accounting explicitly for assigned capacity. Figure 4 reports the capacity-weighted solution.

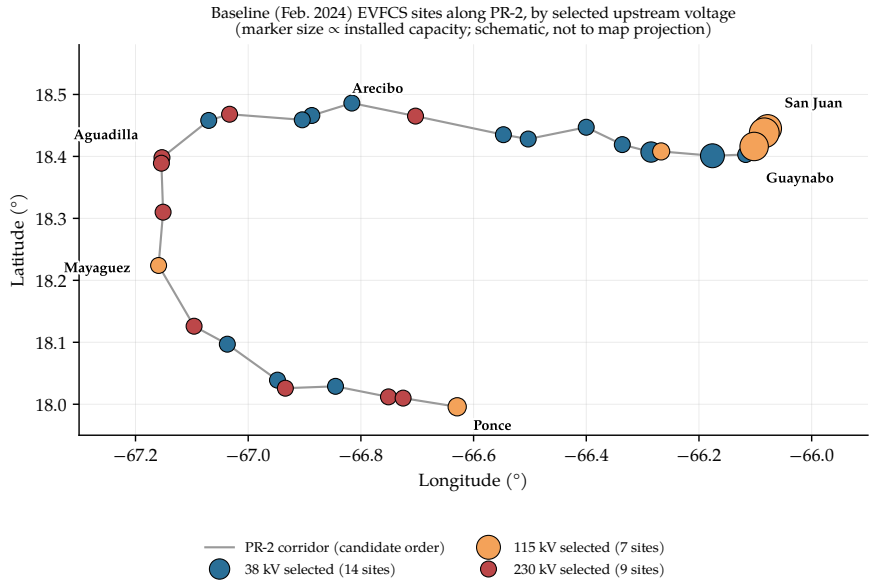


Figure 4. Selected baseline (February 2024) EVFCS sites along PR-2, distinguished by the selected upstream voltage alternative; marker size is proportional to installed charging capacity.

4.2. Primary Scenario Outcomes

Table 5 summarizes the seven primary cases. The observed-stock baseline is feasible, whereas all six future scenarios are infeasible under the full-service formulation. In particular, the calibrated-2030 pathway corresponds to a projected corridor stock of 111,365 electrified vehicles, and its municipal allocations already exceed the candidate-set capacity ceilings in San Juan and Guaynabo.

Table 5. Corridor-wide MILP results. The February 2024 baseline is feasible; all six future cases are infeasible under the full-service model and are therefore characterized by the diagnostic indices $\Delta^\star$ and $\rho^\star$ defined in Section 3.4.

Case	Year	Corridor Stock	Status	$\Delta^\star$	$\rho^\star$	Mun. with Shortfall
Baseline	2024	11,096	Feasible (30 EVFCS, 26.7 MW)	0	0%	—
Calibrated	2030	111,365	Infeasible	1.43	39.4%	2 (Guaynabo, San Juan)
Envelope C	2030	244,670	Infeasible	2.60	53.5%	4
Envelope B	2030	550,508	Infeasible	3.99	64.2%	7
Envelope A	2030	825,762	Infeasible	5.20	69.3%	8
Calibrated	2050	926,408	Infeasible	5.52	70.5%	9
Planning-reference endpoint	2050	1,238,643	Infeasible	6.56	73.9%	11

Both diagnostic indicators increase with the modeled corridor stock: $\Delta^\star$ captures the sum of municipality-level relative shortfalls, whereas $\rho^\star$ measures the share of total corridor charging-energy demand left unmet. Guaynabo and San Juan belong to the shortfall set in every infeasible case, and additional municipalities enter that set as electrification increases.

4.3. Candidate-Set Feasibility and Municipal Shortfall

The diagnostic consistently identifies San Juan and Guaynabo as the first municipalities to exhaust the capacity represented by their candidate sets. PR-2 provides four candidate sites in each municipality; with the adopted 3 MW per-site ceiling, the maximum modeled candidate-set capacity is therefore 12 MW in each municipality. This value is a consequence of the candidate set and station-size bound, not a physical municipal capacity limit. Because candidates are sampled uniformly along PR-2 (Section 2.2), whereas municipal demand is allocated from the full registered stock of each municipality, San Juan and Guaynabo combine few represented candidates with the two largest municipal demand shares in the corridor, 21.8% and 11.4% of the island's baseline registered stock (3868 and 2034 of 17,784 vehicles); their ceilings are therefore reached first. Under the calibrated-2030 pathway, $f_{\mathrm{FC}} = 1$, and $\eta_{\mathrm{use}} = 1$, San Juan requires approximately 60.7 MW of installed charging capacity to satisfy Equation (19), while Guaynabo likewise requires more than its 12 MW candidate-set ceiling. As the electrification level increases, additional municipalities exceed their corresponding candidate-set ceilings.

Applying the candidate-set threshold of Equation (29) (Section 3.4), Table 6 reports the primary thresholds for municipalities appearing in at least one diagnostic shortfall set. San Juan and Guaynabo have the two lowest thresholds, 1.78% and 3.38%, respectively. At the calibrated-2030 level, satisfying the upper-bound demand with stations capped at 3 MW would require at least 21 represented sites in San Juan and 11 in Guaynabo, compared with four candidates in each municipality.

Table 6. Candidate-set capacity ceiling and candidate-set capacity threshold (Equation (29)) for each municipality appearing in the shortfall sets of Table 5, ordered by P_m^{crit}, expressed as a reference-fleet electrification percentage.

Municipality	Candidate Sites $\lvert U_m \rvert$	Ceiling $\overline{X}_m$ (MW)	P_m^{crit} (%)
San Juan	4	12	1.78
Guaynabo	4	12	3.38
Dorado	4	12	9.61
Bayamón	8	24	12.93
Toa Baja	7	21	31.19
Moca	2	6	36.99
Ponce	12	36	37.73
Vega Alta	6	18	52.92
Vega Baja	10	30	73.50
Mayagüez	14	42	85.09
Manatí	9	27	98.60

Summing $r_m(P)$ from Equation (30) over municipalities reproduces the MILP-computed $\Delta^\star$ to four decimal places in all six infeasible future cases. This agreement provides an analytical attribution of the diagnostic shortfall to the municipal candidate-set ceilings under the primary screening assumptions; the paired removal test in Section 4.6 separately evaluates whether the shared upstream-capacity constraint changes that diagnosis.

Although the threshold is only a necessary condition (Section 3.4), for the present candidate set and primary screening assumptions this analytical agreement, together with the paired upstream-capacity benchmark in Section 4.6, identifies the municipal candidate-set ceilings as the binding limits in these scenarios. This agreement need not persist under a finer spatial representation of charging demand.

4.4. Robustness to Drivetrain Definition, Calibration Uncertainty, and Municipal Shares

The published 2030 drivetrain-definition cases—which distinguish BEV-only and plug-in-capable fleet definitions from the broader aggregate registration series—and calibration-uncertainty cases can be evaluated directly against P_m^{crit} without rerunning the MILP [34]. The BEV-only case (4.06%), plug-in-capable case (6.55%), and aggregate bootstrap-derived lower bound (7.9%) all exceed the San Juan and Guaynabo thresholds of 1.78% and 3.38%, respectively. The candidate-set limitation identified for those two municipalities therefore persists across the published 2030 drivetrain definitions and calibration interval.

The assumption of fixed municipal shares can also be examined analytically through Equation (34), evaluated at the calibrated-2030 electrification level $P = 9.0\%$. For San Juan, $q_{\text{SJ}} \leq 1.78/9.0 \approx 0.198$, corresponding to a reduction of at least 80.2% from its baseline municipal share. For Guaynabo, $q_{\text{G}} \leq 3.38/9.0 \approx 0.376$, corresponding to a reduction of at least 62.4%. Under the published calibrated-2030 island-wide trajectory and the remaining planning assumptions, modest perturbations of the baseline municipal shares are therefore insufficient to restore candidate-set feasibility in either municipality.

4.5. Analytical Sensitivity to Fast-Charging Demand and Candidate Capacity

Recent global sensitivity analysis of distribution-grid investment planning has shown that fast-charging-station location and the voltage-limit planning criterion can dominate uncertainty in grid-investment outcomes [47]. The present analysis addresses a different planning layer and uses the closed-form threshold to isolate how the candidate-set feasibility limit varies with its governing demand and capacity parameters. Specifically, Equation (29) exposes the dependence of this limit on assumptions that are otherwise fixed in the primary MILP, through the relations in Equations (31)–(34) (Section 3.4).

At the calibrated-2030 level $P = 9.0\%$ and the primary utilization value $\eta_{\text{use}} = 1$, Equation (31) gives $f_{\text{FC}} \leq 0.198$ for San Juan and $f_{\text{FC}} \leq 0.376$ for Guaynabo. For any lower utilization, these admissible fractions decrease proportionally; for example, the general break-even relations are $f_{\text{FC}} \leq 0.198\eta_{\text{use}}$ for San Juan and $f_{\text{FC}} \leq 0.376\eta_{\text{use}}$ for Guaynabo. These values are not empirical estimates of public fast-charging participation. They are analytical break-even fractions showing how the demand assignment and effective utilization jointly affect the candidate-set ceiling, with all other assumptions held fixed.

The same scaling relationship applies to the station-size ceiling. For $P = 9.0\%$, Equation (32) gives approximately 15.2 MW/site for San Juan and 8.0 MW/site for Guaynabo. These are candidate-set break-even capacities rather than recommended charger-hub sizes; once the station-size ceiling is relaxed, the shared upstream electrical constraint or other omitted network constraints may become limiting.

Candidate-set size can be interpreted similarly through Equation (33). For the calibrated-2030 case, the corresponding multipliers are approximately 5.06 for San Juan and 2.66 for Guaynabo. Because candidate counts are integer, these values correspond to at least 21 represented sites in San Juan and 11 in Guaynabo, consistent with the direct capacity calculation above.

Table 7 summarizes how charging demand, station capacity, candidate-site availability, and utilization affect the candidate-set threshold at the calibrated-2030 level $P = 8.99\%$. Each row changes one assumption from its primary value while all others are held fixed.

The station-size ceiling and the candidate count affect the threshold in Equation (29) linearly, whereas the fast-charging fraction affects it inversely. Halving f_{FC}, doubling $x^{\max}$, or doubling $|U_m|$ therefore produces the same multiplicative change in the threshold, but no single change by a factor of up to three restores candidate-set feasibility in San Juan at this electrification level. The candidate-set multipliers represent hypothetical changes

in the planning discretization; the physical availability and interconnection feasibility of additional sites have not been verified.

Table 7. One-at-a-time analytical sensitivity of the candidate-set feasibility limit at the calibrated-2030 electrification level (P = 8.99%, reported as approximately 9.0% in Table 4), computed from Equation (29). Values are necessary municipal conditions and do not certify feasibility of the complete MILP.

Driver	Tested Value	P_{SJ}^{crit} (%)	P_{G}^{crit} (%)	Municipalities with Shortfall	$\sum_m r_m$ [a]
Primary case	Primary values (Table 2)	1.78	3.38	San Juan, Guaynabo	1.43
Charging demand	$f_{FC} = 0.50$	3.56	6.76	San Juan, Guaynabo	0.85
	$f_{FC} = 0.25$	7.11	13.53	San Juan	0.21
Station capacity	$x^{max} = 6$ MW	3.56	6.76	San Juan, Guaynabo	0.85
	$x^{max} = 9$ MW	5.34	10.15	San Juan	0.41
Candidate-site availability	$2\|U_m\|$	3.56	6.76	San Juan, Guaynabo	0.85
	$3\|U_m\|$	5.34	10.15	San Juan	0.41
Utilization	$\eta_{use} = 0.75$	1.33	2.54	San Juan, Guaynabo, Dorado	1.77
	$\eta_{use} = 0.50$	0.89	1.69	San Juan, Guaynabo, Dorado, Bayamón	2.46
Break-even values at P = 8.99% (San Juan/Guaynabo)					
$f_{FC} \leq 0.198/0.376$; $x^{max} \geq 15.2/8.0$ MW; $\|U_m\| \geq 21/11$ sites; η_{use}: not attainable (would require $\eta_{use} \geq 5.05/2.66 > 1$).					

[a] Sum of municipal shortfall ratios from Equation (30). Values are analytical lower bounds computed from unrounded thresholds and are reported to two decimal places; in the primary case, the sum equals the MILP diagnostic $\Delta^\star = 1.4260$ to four decimal places (Section 4.3).

Utilization cannot restore feasibility, because $\eta_{use} = 1$ is already its most favorable value. Lower utilization instead enlarges the shortfall and, with municipal shares held at their baseline values, extends it to Dorado and Bayamón; these entries are analytical evaluations, not new optimized MILP solutions. The infeasibility diagnosis is therefore robust to the utilization assumption, whereas its magnitude depends on the fast-charging demand assignment.

Finally, the break-even values are necessary conditions for the municipal energy balance, not sufficient conditions for full MILP feasibility. Once a bound is relaxed, corridor coverage, the shared upstream-capacity screen, or network constraints omitted from the model may become limiting, so feasibility under the modified assumptions would have to be confirmed by re-solving the MILP.

4.6. Upstream-Capacity Benchmark Results

Table 8 compares the results obtained with and without the shared upstream-capacity screen. At $\phi_0 = 0.20$, removing this constraint changes neither the feasibility status nor $\Delta^\star$ in any of the seven primary scenarios. Unlike the $\phi = 0.01$ and 0.005 sweep cases in Table 9, these paired runs were not flagged as time-limited.

Table 8. Primary-scenario benchmark with and without the shared upstream-capacity constraint in Equation (18).

Case	Status	$\Delta^\star$, with Screen	$\Delta^\star$, without Screen
Baseline (2024)	Feasible, 30 EVFCS, 26.7 MW	0	0
Calibrated 2030	Infeasible	1.4260	1.4260
Envelope C 2030	Infeasible	2.5976	2.5976
Envelope B 2030	Infeasible	3.9937	3.9937
Envelope A 2030	Infeasible	5.2020	5.2020
Calibrated 2050	Infeasible	5.5232	5.5232
Planning-reference endpoint 2050	Infeasible	6.5628	6.5628

Table 9. Sensitivity of the calibrated-2030 diagnostic shortfall to the upstream-capacity screening fraction ϕ.

ϕ	$\Delta^\star$	Municipalities with Shortfall
0.20	1.43	Guaynabo, San Juan
0.10	1.43	Guaynabo, San Juan
0.05	1.43	Guaynabo, San Juan
0.02	1.52	Bayamón, Dorado, Guaynabo, San Juan
0.01 *	2.60	Bayamón, Dorado, Guaynabo, San Juan, Toa Baja
0.005 *	3.72	Bayamón, Dorado, Guaynabo, San Juan, Toa Baja, Vega Alta

* Solver time limit reached; the reported $\Delta^\star$ and municipality set correspond to the best-found incumbent and are not certified optimal.

The agreement is not interpreted as a statistical result. The MILP is deterministic, and the paired runs compare two formulations under the same demand and planning assumptions rather than independent observations subject to sampling variability; no statistical error variance is therefore associated with the comparison. Determinism does not, however, remove uncertainty in the demand assumptions, candidate-site representation, or available grid capacity; these uncertainties are addressed through the scenario and sensitivity analyses in Sections 4.4 and 4.5 and Table 9.

The comparison therefore establishes that the upstream-capacity screen does not determine the reported diagnostic optimum at $\phi_0 = 0.20$. It does not imply that the constraint has positive slack in every optimal solution or that it is structurally redundant: the sensitivity sweep below shows that the screen begins to affect $\Delta^\star$ when ϕ is reduced to between 0.05 and 0.02. For the feasible baseline, the comparison is limited to feasibility status and $\Delta^\star$.

The calibrated-2030 sensitivity sweep then identifies where an additional upstream-capacity effect begins to appear. As shown in Table 9, $\Delta^\star$ is unchanged for $\phi = 0.20$, 0.10, and 0.05, but increases to 1.52 at $\phi = 0.02$. The transition therefore lies between the tested values $\phi = 0.05$ and $\phi = 0.02$. Results for $\phi = 0.01$ and $\phi = 0.005$ are reported only as best-found incumbents because the solver reached its time limit.

Finally, removing the municipal-access condition in Equation (21) from the baseline leaves the solution unchanged at 30 EVFCS and 26.7 MW. Every corridor municipality already requires positive installed capacity to satisfy its own baseline demand, so the explicit one-station minimum is redundant for the full-service baseline under the present candidate set.

4.7. Robustness of the Diagnostic Objective

Because $\Delta^\star = \sum_m \xi_m / D_m$ weights municipal shortfalls in relative rather than absolute terms, the calibrated-2030 diagnostic was also evaluated using a lexicographic minimax formulation that first minimizes the maximum municipal relative shortfall,

$$\theta^\star = \min\ \theta \quad \text{s.t.} \quad \xi_m \le \theta D_m,\ \forall m \in M, \tag{36}$$

and then minimizes the original sum-relative objective of Equation (26) over the resulting minimax-optimal set, holding $\theta \le \theta^\star + \varepsilon$. The tolerance $\varepsilon = 10^{-8}$ preserves the first-stage minimax optimum numerically. For the calibrated-2030 case, $\theta^\star = 0.802169$, equal to San Juan's shortfall ratio under the primary sum-relative diagnostic. The second stage returns $\Delta^\star = 1.425959$ and $\rho^\star = 0.393978$, identical to the primary diagnostic to six decimal places, with the same shortfall set (Guaynabo, San Juan) and the same municipal shortfall values (477,531 and 1,167,788 kWh/day, respectively). The identical results under both objectives confirm that the calibrated-2030 shortfall pattern is not driven by the choice of shortfall-aggregation objective.

5. Discussion

5.1. Planning Implications of the Identified Feasibility Limit

At the primary planning values, the modeled feasibility limit is governed by the interaction between municipal charging demand, the number of represented candidate sites, and the 3 MW per-site ceiling. San Juan and Guaynabo exhaust the capacity represented by their PR-2 candidate sets, and at $\phi_0 = 0.20$ the shared upstream-capacity screen does not determine the diagnostic optimum. The limiting condition is therefore specific to the adopted candidate set and station-size ceiling; expanding the candidate set, allowing larger hubs, or incorporating off-corridor locations could change which constraint becomes binding first.

Corridor coverage and local charging capacity are separate requirements: a route can satisfy the corridor-coverage constraint while still providing too little modeled charging capacity in municipalities where demand is concentrated. For PR-2, candidate-set expansion in the most constrained urban areas should therefore be examined before interpreting infeasibility as evidence that upstream line capacity is the immediate limiting factor. This sequencing separates a limitation of the represented charging-infrastructure options from subsequent power-system questions and motivates the separate assessment of upstream-capacity screening and generation adequacy that follows.

The proposed feasibility diagnostic provides a planning-level tool to inform sustainable transport-electrification policies by distinguishing candidate-site capacity limitations from the electrical constraints represented in the model. The findings have different implications for the two planning communities, as summarized in Table 10. For transportation and charging-infrastructure planners, the central finding is a mismatch between where registered demand is concentrated and where candidate capacity is represented: San Juan and Guaynabo hold 33.2% of the island's baseline registered stock used for demand allocation, whereas only 8 of the 229 candidates represented along PR-2 lie within them. Before additional siting decisions are made for the metropolitan area, the candidate representation should therefore be broadened, through denser or off-corridor candidates, and the screening value $f_{FC} = 1$ should be replaced by observed fast-charging participation once such data become available. The site counts and break-even capacities in Table 7 quantify the scale of the gap; they are not verified site inventories or recommended hub sizes.

Table 10. Translation of the main findings into planning implications. All findings refer to the adopted corridor-planning representation and primary assumptions.

Finding	Planning Implication	Primary Decision-Maker
San Juan and Guaynabo: 33.2% of the island's registered stock used for demand allocation; 4 of the 229 PR-2 candidates each	Broaden or refine the metropolitan candidate representation (denser or off-corridor sites) before further siting	Transportation authorities; charging-infrastructure planners
Candidate-set thresholds of 1.78% and 3.38%, below the calibrated-2030 level of 8.99%	Use the thresholds as early-warning levels at which represented capacity is exhausted under the stated assumptions	Charging-infrastructure and energy-policy planners

Table 10. *Cont.*

Finding	Planning Implication	Primary Decision-Maker
At least 21 and 11 represented 3 MW sites, or 15.2 and 8.0 MW/site, at the calibrated-2030 level	Indicates the scale of a hypothetical expansion; not a verified site inventory or recommended hub size	Charging-infrastructure planners
Upstream screen does not determine the diagnostic optimum at $\phi_0 = 0.20$; its effect appears between $\phi = 0.05$ and 0.02	Obtain utility-certified segment margins; begin detailed interconnection studies in the first limiting municipalities	Utility and power-system planners
Infeasibility robust to η_{use}; magnitude sensitive to f_{FC}	Collect observed fast-charging participation and utilization data to replace the screening values	Transportation agencies; charging operators

For power-system planners, the model is a pre-screening tool rather than an interconnection assessment. At $\phi_0 = 0.20$, the shared upstream-capacity screen does not determine the reported diagnostic optimum, but the sensitivity sweep shows that its influence appears when the screening fraction is reduced to between 0.05 and 0.02. Utility-certified segment margins are therefore the first input needed to confirm or revise this result. The municipalities that become limiting first suggest a diagnostic order in which detailed studies could begin: San Juan and Guaynabo, followed by Dorado and Bayamón as electrification increases. This order is not a validated ranking of reinforcement urgency, which would also depend on existing loads, substation conditions, and observed charging demand. Such studies, including feeder and substation loading, AC power flow, protection, voltage, reliability, and reinforcement analysis, remain outside the scope of the present model and are not replaced by it.

5.2. Grid-Capacity Screening and Generation Adequacy

The fact that removing the shared upstream-capacity screen does not change the diagnostic optimum at $\phi_0 = 0.20$ does not imply that Puerto Rico's power system can supply the modeled charging demand. Equation (18) is only a thermal-capacity screening proxy associated with candidate locations. The model does not represent generation adequacy, AC power flow, voltage, reactive power, protection, short-circuit duty, or contingencies. Recent resource-adequacy proceedings report 6290 MW of installed thermal nameplate capacity and 4108 MW of dependable thermal capacity for 2026, together with recurrent load shedding and emergency-generation measures [29–32]. These 2026 capacity values are included only as contemporary system context and are not assumed to represent available generation in the 2030 or 2050 scenarios.

The magnitude of the modeled charging-energy requirement also illustrates why generation adequacy remains an important follow-on question. Under the primary upper-bound assumption of one 37.5 kWh fast-charging event per modeled vehicle per day, the calibrated-2030 corridor stock corresponds to approximately 4.18 GWh/day, or 174 MW if distributed uniformly over 24 h. The calibrated-2050 case corresponds to approximately 34.7 GWh/day, equivalent to an average of 1.45 GW. These quantities are energy-to-average-power conversions rather than generation-capacity requirements because the present model does not represent hourly charging coincidence, existing system load, generator availability, reserves, renewable output, or storage. They nevertheless illustrate that generation ade-

quacy warrants explicit evaluation as electrification increases, even when the upstream thermal-capacity screen does not determine the diagnostic optimum. Assessing generation adequacy under Puerto Rico's renewable-energy transition remains a separate requirement for evaluating the broader sustainability of transport electrification.

The proposed framework therefore provides an initial planning layer: corridor-wide feasibility and candidate-set limitations are screened first, while subsequent studies may refine charging demand using traffic- and behavior-based profiles and evaluate distribution-network reinforcement [11]. Within the corridor-planning model and at $\phi_0 = 0.20$, the benchmark therefore shows that the shared upstream-capacity screen is not the first limiting constraint; it does not establish system-level readiness for the resulting EV load.

5.3. Comparison with Published EVFCS Planning Studies

Published EVFCS planning studies vary considerably in spatial scale, demand representation, and electrical detail. Highway-oriented optimization models address corridor-focused station location [22]; joint location, capacity, and demand allocation through MILP formulations [21]; and traffic-based probabilistic demand estimation combined with station sizing and distribution-grid reinforcement assessment [11]. Coupled transportation–power models incorporate explicit electrical-network constraints [14], while robust-siting models show that spatial service limits can themselves become binding [26]. Island studies provide complementary system and spatial perspectives [3,7,18,48]. Table 11 places the present formulation within this methodological range. Its distinguishing analytical elements are the paired with/without-upstream-capacity-screen test and the closed-form candidate-set feasibility threshold, which together separate two potential sources of infeasibility within the adopted screening model.

Table 11. Comparison of methodological features with selected EVFCS planning studies.

Study	System	Spatial Unit	Grid Representation	Demand/Adoption Input	Upstream-Screen Removal
Present study	Puerto Rico, PR-2	229 corridor sites	Shared screened segment capacity	Baseline + 6 future cases	Yes (7 cases)
Le et al. [17]	Phu Quoc Island	16-bus, 22 kV network	AC power flow with an $N-1$ contingency criterion (loss of one modeled component)	Single planning horizon	Not reported
Jovanovic et al. [21]	U.S. I-70 and I-95 corridors	Highway candidate sites	Station-capacity and service constraints; no explicit power-network model	Multiple EV-adoption scenarios	Not reported
Anadón Martínez et al. [11]	Norwegian E18–E39 highway corridor	Predefined high-traffic locations	Detailed medium-voltage grid reinforcement assessment with transformer, line, and battery alternatives	Probabilistic demand from traffic, mileage, state of charge, and return-time data	Not reported
García García et al. [7]	Canary Islands	Archipelago-wide	Aggregate energy and peak-load representation	2025/2030/2040 scenarios	Not reported
Zhang et al. [14]	Coupled highway–power network	Transportation nodes and distribution network	Explicit distribution-network operating constraints	Plug-in electric-vehicle population sensitivity	Not reported

AC, alternating current.

These studies illustrate the trade-off between model detail and feasibility diagnosis. Traffic- and probability-based approaches [11] represent charger use more realistically and, in the cited study, include a detailed medium-voltage reinforcement assessment; however, they start from predefined high-traffic locations and are not designed to attribute

infeasibility to the capacity of a municipal candidate set. Coupled transportation–power and AC power-flow models [14,17] offer the greatest electrical detail but require network data, such as impedances, loading, and contingency information, that are rarely available for every candidate site along a 27-municipality corridor. Highway MILP formulations [21,22] share the discrete siting and capacity decisions of the present model, but they focus on finding covering or balanced deployments rather than on explaining why full service cannot be achieved. Archipelago-scale assessments [7] capture system-wide energy and peak-load effects without resolving individual station sites.

The present formulation does not represent traffic-based demand or AC network detail; it focuses instead on a municipal infeasibility diagnostic, a closed-form threshold that reproduces the diagnostic shortfall, and a paired test that isolates the upstream-capacity screen. These differences reflect the scope of each method rather than general superiority; in particular, the framework does not establish physical interconnection feasibility, which AC-based approaches are better suited to assess.

5.4. Transferability and Limitations

The formulation is intended for planning-level screening, not interconnection approval or operational analysis. Its principal electrical limitation is that upstream capability is represented only through screened segment thermal capacity, whereas detailed coupled-network and hosting-capacity studies explicitly represent power-system operating constraints and, in some cases, time-varying load profiles [14,16]. Generation adequacy, AC power flow, voltage, reactive power, protection, short-circuit duty, and the $N-1$ contingency criterion remain outside the model. Unity power factor is likewise assumed; because pf enters the thermal-capacity screen multiplicatively with ϕ_e, moderate departures from unity power factor are represented by an equivalent change in the effective screening fraction. Harmonic distortion and other AC power-quality effects of DC fast-charger inverters are not modeled.

Spatially, candidate sites are discretized at approximately 1 km along PR-2 and each site is capped at 3 MW; off-corridor sites, denser candidate generation, and larger hubs are not represented. Alternative corridor-discretization resolutions were not evaluated, so the reported candidate-set thresholds characterize the adopted 1 km representation and should not be interpreted as intrinsic physical limits of the corresponding municipalities. The candidate-set multipliers in Table 7 indicate the scale of the change in representation that would be required, but they do not replace re-solving the model with an alternative discretization or verified site inventory. The four-decimal agreement between the analytical and MILP shortfalls also relies on the present aggregate municipal-demand representation and need not persist if charging demand is spatially resolved within each municipality. In addition, the primary experiments apply a uniform screening fraction across the 38, 115, and 230 kV layers. Actual available-capacity margins may differ by voltage class and network condition, and differentiated values of ϕ_e would require utility-certified information not available for the present candidate set.

The demand model is intentionally aggregate and does not resolve trip patterns, arrival times, state of charge, or time-varying charging coincidence; traffic-based probabilistic studies show that these factors can materially alter both the timing and magnitude of highway fast-charging peaks [11]. In addition, future island-wide stocks are allocated according to baseline municipal shares, so the formulation does not capture future migration, changes in the geography of vehicle ownership, or trip-based redistribution of charging demand. The analytical sensitivity analysis in Section 4.4 shows that calibrated-2030 candidate-set feasibility would require reductions of approximately 80.2% and 62.4% in the baseline shares of San Juan and Guaynabo, respectively. The primary demand screen also uses $f_{\mathrm{FC}} = 1$, assigning one representative 150 kW, 15 min event per modeled vehicle per day. Section 4.5 therefore

reports demand–utilization break-even relations, rather than treating the upper-bound assignment as behavioral truth; because feasibility depends on η_{use}/f_{FC}, lower effective utilization proportionally lowers the admissible fast-charging demand fraction. Queueing, heterogeneous charging frequency, home charging, and managed charging also remain outside the model. A future extension should replace the aggregate-stock screen with a travel-energy and charging-schedule formulation; related geospatial energy-allocation and charging-schedule methods have been applied to medium- and heavy-duty electrification in Puerto Rico under the PR100 initiative [43].

The registration series itself is broader than a BEV-only fleet, so the aggregate-stock case should be interpreted as an upper-bound screening input. Published drivetrain and calibration cases are checked analytically against P_m^{crit}, but the reference-fleet-size sensitivity is not rerun through the corridor-wide MILP. In addition, results for $\phi \leq 0.01$ are exploratory because the solver time limit is reached, and the 100% 2050 endpoint is a planning stress case rather than a statutory vehicle-fleet target.

Within these limitations, the formulation can be applied to other corridors when comparable candidate-site, zonal-demand, and upstream-network data are available. The threshold P_m^{crit} can be evaluated before optimization as a rapid screening test for candidate-set infeasibility and can help determine whether expanding the candidate set should precede a more computationally detailed planning analysis.

6. Conclusions

To inform sustainable transport electrification in Puerto Rico, this study examined when a corridor-wide EV fast-charging plan for Puerto Rico Highway 2 (PR-2) ceases to be feasible under the adopted planning representation, which modeled constraint becomes limiting first, and how that limit depends on the main planning assumptions. The February 2024 observed-stock baseline is feasible with 30 EVFCS, 178 ports, and 26.7 MW of installed capacity, whereas all six future electrification cases are infeasible under the primary upper-bound demand assignment, the adopted candidate set, and the 3 MW per-site ceiling. In the calibrated-2030 case (8.99% reference-fleet electrification), the diagnostic returns $\Delta^\star = 1.4260$, the sum of municipal relative shortfalls, and $\rho^\star = 39.4\%$, the fraction of modeled corridor charging energy that cannot be served.

Under the primary planning assumptions, the first limiting constraint is the charging capacity represented by the candidate sets of San Juan and Guaynabo. These municipalities hold 33.2% of the island's registered stock used for demand allocation but are represented by four PR-2 candidates each, and their candidate-set thresholds of 1.78% and 3.38% lie below every published 2030 case, including the BEV-only definition (4.06%). The analytical shortfall reproduces the MILP diagnostic to four decimal places in all six infeasible cases, and the lexicographic minimax variant returns the same shortfall pattern. At $\phi_0 = 0.20$, removing the shared upstream-capacity screen changes neither feasibility nor $\Delta^\star$ in any of the seven primary cases, which indicates that the candidate-set capacity becomes limiting before the upstream screen at this screening level; the screen begins to affect the diagnostic only when the screening fraction is reduced to between 0.05 and 0.02.

The sensitivity analysis further shows that the fast-charging fraction, the station-size ceiling, and the candidate count shift the threshold by the same multiplicative factor, but no single change up to threefold restores candidate-set feasibility in San Juan at the calibrated-2030 level. Doing so would require $f_{FC} \leq 0.198$ in San Juan and $f_{FC} \leq 0.376$ in Guaynabo, per-site ceilings of approximately 15.2 and 8.0 MW, or at least 21 and 11 represented 3 MW sites, compared with four in each municipality. Because $\eta_{use} = 1$ is already the most favorable utilization value, utilization alone cannot restore feasibility. These are analytical break-

even conditions, not recommended station sizes, verified site inventories, or guarantees of full-model feasibility.

In short, under the primary planning assumptions, the PR-2 plan becomes infeasible because the represented candidate sets cannot accommodate the required charging capacity, rather than because of the shared upstream-capacity screen. These conclusions depend on the adopted corridor discretization, station-size limit, demand assignment, municipal allocation, and electrical-screening assumptions, and they do not establish power-system readiness or utility interconnection feasibility, nor do they assess lifecycle emissions or economic costs. Within those limits, the framework provides a staged feasibility-screening approach to inform infrastructure decisions supporting sustainable transport electrification: it indicates whether spatial charging-infrastructure limitations should be addressed before detailed network and generation studies are undertaken. Future work should expand the candidate set beyond the immediate PR-2 corridor, examine larger hubs and complementary corridors, replace the aggregate-stock demand screen with trip- and time-dependent charging demand, update the baseline as comparable municipal data become available, and couple the spatial framework with explicit distribution-network and generation-adequacy analyses.

Author Contributions: Conceptualization, G.A.F.-C.; methodology, G.A.F.-C. and D.D.C.-O.; software, G.A.F.-C. and D.D.C.-O.; validation, G.A.F.-C., D.D.C.-O., A.C.L.-H. and F.A.-R.; formal analysis, D.D.C.-O., A.C.L.-H. and A.I.-R.; investigation, G.A.F.-C., D.D.C.-O. and A.I.-R.; resources, F.A.-R.; data curation, G.A.F.-C. and D.D.C.-O.; writing—original draft preparation, G.A.F.-C.; writing—review and editing, D.D.C.-O., A.C.L.-H. and F.A.-R.; visualization, A.C.L.-H.; supervision, D.D.C.-O., A.C.L.-H., A.I.-R. and F.A.-R.; project administration, A.C.L.-H. and A.I.-R. All authors have read and agreed to the published version of the manuscript.

Funding: This research received no external funding.

Institutional Review Board Statement: Not applicable.

Informed Consent Statement: Not applicable.

Data Availability Statement: The annual Puerto Rico registered electrified-vehicle stock series used to calibrate the published generalized-logistic pathway is reported in Table 2 of Feo-Cediel et al. [34]. The underlying Department of Transportation and Public Works records remain subject to applicable data-use restrictions. The processed municipal inputs, scenario data, and optimization code supporting the present study are available from the corresponding author upon reasonable request.

Conflicts of Interest: The authors declare no conflicts of interest.

Abbreviations

The following abbreviations are used in this manuscript:

AC	Alternating Current
BEV	Battery Electric Vehicle
CBC	COIN-OR Branch and Cut
DC	Direct Current
DTOP	Puerto Rico Department of Transportation and Public Works
EV	Electric Vehicle
EVFCS	Electric Vehicle Fast-Charging Station
FID	Feature Identifier
GIS	Geographic Information System
MILP	Mixed-Integer Linear Programming
NEVI	National Electric Vehicle Infrastructure
PR-2	Puerto Rico Highway 2
PR100	Puerto Rico Grid Resilience and Transitions to 100% Renewable Energy Study

Appendix A. Computational Procedure

Algorithm A1 summarizes the computational procedure used for scenario evaluation, feasibility diagnosis, and robustness testing described in Section 3.

Algorithm A1 Corridor-wide EVFCS planning and feasibility-diagnostic procedure

Require: Candidate sites U, municipalities M, upstream segments E; observed stocks $N_{m,0}$; municipal shares s_m; scenario q with island-wide stock S_q; model parameters; screening fractions ϕ_e; minimax tolerance $\varepsilon = 10^{-8}$

Ensure: Feasibility status, selected configuration or diagnostic shortfalls, candidate-set thresholds, and optimality-certification status

if q is the observed-stock baseline **then**
  Set $N_{m,q} = N_{m,0}$
else
  Compute $N_{m,q} = s_m S_q$
end if
Compute $D_m = f_{\mathrm{FC}} E_{\mathrm{s}} N_{m,q}$
Compute S_e, $C_e(\phi_e)$, and $\overline{P}^{\mathrm{loss}}_{ue}$ from Equations (5)–(9)
Build the full-service corridor-wide MILP
Stage 1: minimize $\sum_{u \in U} x_u$ and solve
if Stage 1 returns a feasible solution **then**
  if optimality is certified **then**
    Set $X^{\mathrm{ref}} = X^{\star} = \sum_{u \in U} x_u$
  else
    Set $X^{\mathrm{ref}} = X^{\mathrm{inc}} = \sum_{u \in U} x_u$ and flag the solution as not optimality-certified
  end if
  Fix $\sum_{u \in U} x_u = X^{\mathrm{ref}}$
  Stage 2: minimize $\sum_{u \in U} \sum_{e \in E_u} (\overline{P}^{\mathrm{loss}}_{ue} / x^{\max}) x_{ue}$
  Store the site–segment configuration and set $\Delta^{\star} = \rho^{\star} = 0$
else if Stage 1 is certified infeasible **then**
  Introduce $\xi_m \geq 0$, $\forall m \in M$
  Minimize $\sum_{m \in M} \xi_m / D_m$
  Store $\Delta^{\star}$, $\rho^{\star}$, and ξ_m
else
  Record the run as unresolved and do not interpret it as infeasible
end if
for each municipality $m \in M$ **do**
  Compute P^{crit}_m from Equation (29)
end for
Repeat each primary scenario without the shared upstream-capacity constraint and compare feasibility status and $\Delta^{\star}$
For calibrated 2030, repeat the diagnostic for the prescribed uniform screening levels $\phi_e = \phi$, $\forall e \in E$
if q is calibrated 2030 and the full-service MILP is infeasible **then**
  Minimax D1: minimize θ subject to $\xi_m \leq \theta D_m$, $\forall m \in M$
  Fix $\theta \leq \theta^{\star} + \varepsilon$
  Minimax D2: minimize $\sum_{m \in M} \xi_m / D_m$
  Compare $\Delta^{\star}$, $\rho^{\star}$, and the shortfall set with the primary diagnostic
end if
if q is the feasible baseline **then**
  Repeat Stage 2 with the audit-only objective $\sum_{u \in U} \sum_{e \in E_u} \overline{P}^{\mathrm{loss}}_{ue} z_{ue}$
  Compare selected sites, upstream assignments, and port allocation with the capacity-weighted solution
end if
Export selected locations and diagnostic results for GIS inspection

References

1. International Energy Agency. Global EV Outlook 2024. Available online: https://www.iea.org/reports/global-ev-outlook-2024 (accessed on 22 May 2026).
2. Irfan, M.; Tahir, T.; Deilami, S.; Huang, S.; Veettil, B.P. A Novel Predictive Strategy for Daily Energy Cost Reduction in Solar "PV + EV" System with V2G and V2H Modes. In *Proceedings of the 2025 IEEE International Conference on Energy Technologies for Future Grids (ETFG)*; IEEE: Piscataway, NJ, USA, 2025; pp. 1–6. [CrossRef]
3. O'Neill-Carrillo, E.; Lave, M.; Haines, T. Systemwide Considerations for Electrification of Transportation in Islands and Remote Locations. *Vehicles* **2021**, *3*, 498–511. [CrossRef]
4. Mastoi, M.S.; Zhuang, S.; Munir, H.M.; Haris, M.; Hassan, M.; Usman, M.; Bukhari, S.S.H.; Ro, J.S. An in-depth analysis of electric vehicle charging station infrastructure, policy implications, and future trends. *Energy Rep.* **2022**, *8*, 11504–11529. [CrossRef]
5. Unterluggauer, T.; Rich, J.; Andersen, P.B.; Hashemi, S. Electric vehicle charging infrastructure planning for integrated transportation and power distribution networks: A review. *eTransportation* **2022**, *12*, 100163. [CrossRef]
6. Acharige, S.S.G.; Haque, M.E.; Arif, M.T.; Hosseinzadeh, N.; Hasan, K.N.; Oo, A.M.T. Review of Electric Vehicle Charging Technologies, Standards, Architectures, and Converter Configurations. *IEEE Access* **2023**, *11*, 41218–41255. [CrossRef]
7. García García, A.; Rubio Matilla, V.; López Arquillo, J.D.; Oliveira, C. Feasibility of Large-Scale Electric Vehicle Deployment in Islanded Grids: The Canary Islands Case. *Electronics* **2025**, *14*, 4579. [CrossRef]
8. Charly, A.; Foley, A.; Caulfield, B. Identifying optimal locations for community electric vehicle charging. *Sustain. Cities Soc.* **2023**, *94*, 104573. [CrossRef]
9. Catalbas, M.C.; Yildirim, M.; Gulten, A.; Kurum, H. Estimation of optimal locations for electric vehicle charging stations. In *Proceedings of the 2017 IEEE International Conference on Environment and Electrical Engineering and 2017 IEEE Industrial and Commercial Power Systems Europe (EEEIC / I&CPS Europe)*; IEEE: Piscataway, NJ, USA, 2017; pp. 1–4. [CrossRef]
10. Asamer, J.; Reinthaler, M.; Ruthmair, M.; Straub, M.; Puchinger, J. Optimizing charging station locations for urban taxi providers. *Transp. Res. Part A Policy Pract.* **2016**, *85*, 233–246. [CrossRef]
11. Anadón Martínez, V.; Sumper, A.; Saldaña-Gonzalez, A.E.; Gadelha, V. Planning Fast-Charging Stations along Highways Using Probability Distribution Functions and Traffic Data. *Sustain. Energy Technol. Assess.* **2025**, *82*, 104547. [CrossRef]
12. Shukla, A.; Verma, K.; Kumar, R. Multi-Objective Synergistic Planning of EV Fast Charging Stations in Distribution System Coupled with Transportation Network. *IET Gener. Transm. Distrib.* **2019**, *13*, 3421–3432. [CrossRef]
13. Islam, M.M.; Shareef, H.; Mohamed, A. Optimal Location and Sizing of Fast Charging Stations for Electric Vehicles by Incorporating Traffic and Power Networks. *IET Intell. Transp. Syst.* **2018**, *12*, 947–957. [CrossRef]
14. Zhang, H.; Moura, S.J.; Hu, Z.; Song, Y. PEV Fast-Charging Station Siting and Sizing on Coupled Transportation and Power Networks. *IEEE Trans. Smart Grid* **2018**, *9*, 2595–2605. [CrossRef]
15. Zeb, M.Z.; Imran, K.; Khattak, A.; Janjua, A.K.; Pal, A.; Nadeem, M.; Zhang, J.; Khan, S. Optimal Placement of Electric Vehicle Charging Stations in the Active Distribution Network. *IEEE Access* **2020**, *8*, 68124–68134. [CrossRef]
16. Bragatto, T.; Carere, F.; Cresta, M.; Gatta, F.M.; Geri, A.; Maccioni, M.; Paulucci, M. Developing a Public EV Charging Infrastructure in a DSO's Perspective: Hosting Capacity Assessment and Grid Reinforcements on a Real Case Study. *Electr. Power Syst. Res.* **2023**, *221*, 109463. [CrossRef]
17. Le, T.M.C.; Nguyen, T.K.; Le, T.N. Grid-Impact-Aware Planning of Electric Vehicle Charging Infrastructure for a Tourism-Intensive Island Grid Using Mixed-Integer Optimization and AC Power Flow Assessment. *IEEE Access* **2026**, *14*, 119449–119466. [CrossRef]
18. Clairand, J.M.; Álvarez Bel, C.; Rodríguez-García, J.; Escrivá-Escrivá, G. Impact of Electric Vehicle Charging Strategy on the Long-Term Planning of an Isolated Microgrid. *Energies* **2020**, *13*, 3455. [CrossRef]
19. Chae, S.H.; Kim, G.H.; Choi, Y.J.; Kim, E.H. Design of Isolated Microgrid System Considering Controllable EV Charging Demand. *Sustainability* **2020**, *12*, 9746. [CrossRef]
20. Schettini, T.; dell'Amico, M.; Fumero, F.; Jabali, O.; Malucelli, F. Locating and Sizing Electric Vehicle Chargers Considering Multiple Technologies. *Energies* **2023**, *16*, 4186. [CrossRef]
21. Jovanovic, R.; Bayhan, S.; Bayram, I.S. Optimizing Electric Vehicle Charging Infrastructure on Highways: A MILP Model for Balanced Demand Allocation. *Int. J. Energy Res.* **2026**, *2026*, 9945830. [CrossRef]
22. Erdoğan, S.; Çapar, İ.; Çapar, İ.; Motalleb Nejad, M. Establishing a Statewide Electric Vehicle Charging Station Network in Maryland: A Corridor-Based Station Location Problem. *Socio-Econ. Plan. Sci.* **2022**, *79*, 101127. [CrossRef]
23. Ghanbari Motlagh, S.; Li, L. A Review on Electric Vehicle Charging Station Planning: Infrastructure Placement, Sizing, Upgrades, and Uncertainties. *J. Energy Storage* **2026**, *141*, 119325. [CrossRef]
24. Ferraz, R.S.F.; Ferraz, R.S.F.; Rueda-Medina, A.C. Optimized Planning for Electric Vehicle Charging Stations: A Systematic Review. *IEEE Access* **2025**, *13*, 157059–157080. [CrossRef]
25. Guo, C.; Yang, J.; Yang, L. Planning of Electric Vehicle Charging Infrastructure for Urban Areas with Tight Land Supply. *Energies* **2018**, *11*, 2314. [CrossRef]

26. Wang, K.; Sun, T.; Xu, H.; Sy, C.L. Robust Optimisation for Electric Vehicle Charging Station Siting Under Demand Uncertainty: A Multi-Station Network Planning Model. *Process Integr. Optim. Sustain.* **2026**. [CrossRef]
27. Kwasinski, A.; Andrade, F.; Castro-Sitiriche, M.J.; O'Neill-Carrillo, E. Hurricane Maria Effects on Puerto Rico Electric Power Infrastructure. *IEEE Power Energy Technol. Syst. J.* **2019**, *6*, 85–94. [CrossRef]
28. National Renewable Energy Laboratory. *Puerto Rico Grid Resilience and Transitions to 100% Renewable Energy Study (PR100)*; Technical Report; NREL: Golden, CO, USA, 2024. Available online: https://catalog.data.gov/dataset/pr100-puerto-rico-grid-resilience-and-transition-to-100-renewable-energy (accessed on 21 October 2026).
29. Puerto Rico Energy Bureau. Motion to Submit LUMA's Fiscal Year 2026 Resource Adequacy Study, 2026. Case No. NEPR-MI-2022-0002. Available online: https://energia.pr.gov/wp-content/uploads/sites/7/2026/01/20251205-MI20220002-Motion-to-Submit-LUMAs-Fiscal-Year-2026-Resource-Adequacy-Study.pdf (accessed on 21 October 2026).
30. LUMA Energy. LUMA's Updated Position Regarding Additional Temporary Generation: Interim Update for Summer 2026, 2026. Filed September 4, 2026, Case No. NEPR-MI-2024-0005. Available online: https://energia.pr.gov/wp-content/uploads/sites/7/2026/09/20260904-MI20240005-Motion-Submitting-LUMAs-Updated-Position-Regarding-Temporary-Generation.pdf (accessed on 21 October 2026).
31. U.S. Department of Energy. Puerto Rico Generation 202(c) Emergency Order No. 202-25-1E, 2026. Renewed August 10, 2026, in Effect Through November 7, 2026, Under Section 202(c) of the Federal Power Act. Available online: https://www.energy.gov/documents/doe-order-no-202-25-1e (accessed on 21 October 2026).
32. Institute for Energy Economics and Financial Analysis (IEEFA). *Fossil Fuel Generation Threatens Puerto Rico's Climate Goals*; Technical Report; IEEFA: Valley City, OH, USA, 2026. Available online: https://ieefa.org/sites/default/files/2026-05/English%20version_Puerto%20Rico%20Fossil%20Fuels_April%202026.pdf (accessed on 21 October 2026).
33. Domarchi, C.; Cherchi, E. Electric Vehicle Forecasts: A Review of Models and Methods Including Diffusion and Substitution Effects. *Transp. Rev.* **2023**, *43*, 1118–1143. [CrossRef]
34. Feo-Cediel, G.A.; Luna, A.C.; Irizarry Rivera, A.; Andrade, F.; Campo-Ossa, D.D. Assessing planning-reference electrification envelopes against a calibrated EV-diffusion trajectory in Puerto Rico. *Discov. Veh.* **2026**, *2*, 33. [CrossRef]
35. Puerto Rico Department of Transportation and Public Works (DTOP); San Juan, PR, USA; Puerto Rico Department of Treasury; San Juan, PR, USA. Electric Vehicle Import and Registration Data, 2014-February 2024. Unpublished Internal Dataset Including Records of Electric Vehicle Imports Since the Enactment of Law 81-2014. 2025.
36. GIS Puerto Rico. Puerto Rico Electrical Infrastructure—Geospatial Data, 2024. Available online: https://gis.pr.gov/descargaGeodatos/Infraestructuras/Pages/Electricidad.aspx (accessed on 12 March 2025).
37. Government of Puerto Rico. Act No. 17-2019: Puerto Rico Energy Public Policy Act. 2019; Approved 11 April 2019. Available online: https://bvirtualogp.pr.gov/ogp/Bvirtual/leyesreferencia/PDF/2-ingles/17-2019.pdf (accessed on 21 October 2026).
38. Government of Puerto Rico. Act No. 33-2019: Puerto Rico Climate Change Mitigation, Adaptation, and Resilience Act. 2019; Approved 22 May 2019. Available online: https://bvirtualogp.pr.gov/ogp/Bvirtual/leyesreferencia/PDF/33-2019.pdf (accessed on 21 October 2026).
39. Government of Puerto Rico. Act No. 81-2014: Law for the Promotion of Vehicles Primarily Powered by Electricity. 2014; Approved 2 July 2014. Available online: https://bvirtualogp.pr.gov/ogp/Bvirtual/leyesreferencia/PDF/2-ingles/0081-2014.pdf (accessed on 21 October 2026).
40. Chu, J.; Gilmore, B.; Hassol, J.; Jenn, A.; Lommele, S.; Myers, L.; Richardson, H.; Schroeder, A.; Shah, M. *National Electric Vehicle Infrastructure Formula Program Annual Report: Plan Year 2022–2023*; Technical Report; National Renewable Energy Laboratory (NREL): Golden, CO, USA, 2023. [CrossRef]
41. Thrash, R.; Nuckles, K.; Murrah, A.; Lancaster, M. *Overhead Conductor Manual*, 2nd ed.; Southwire Company: Carrollton, GA, USA, 2007.
42. Brugg Cables. Technical User Guide HV XLPE Cable Systems. 2020. Available online: https://www.cabledatasheet.com/pdf/Technical_User_Guide_HV_XLPE_Cable_Systems_EN.pdf (accessed on 1 May 2025).
43. Moog, E.; Mammoli, A.; Garrett, R.; Lave, M. *PR100: Estimated Medium- and Heavy-Duty Electric Vehicle Adoption and Load Estimation in Puerto Rico Through 2050*; Technical Report SAND2023-14443, OSTI ID: 2349515; Sandia National Laboratories: Albuquerque, NM, USA, 2023. [CrossRef]
44. Puerto Rico Department of Transportation and Public Works (DTOP). Total de Vehículos con marbete activo al 30 de junio de 2026. Municipality-Level Summary Distributed by the Puerto Rico Institute of Statistics. Available online: https://www.estadisticas.pr.gov/en-us/productos/registro-de-vehiculos-de-motor-por-municipios-y-por-categorias (accessed on 14 October 2026).
45. Katsh, G. Illustrative Highway Service Plaza Charging Needs (National Grid). GridWise Alliance Workshop: Grid Integration of EV Charging Infrastructure, 14 March 2022. Available online: https://gridwise.org/wp-content/uploads/2022/03/EV-Workshop-Slides-3.14.22.pdf (accessed on 14 October 2026).
46. Marler, R.T.; Arora, J.S. Survey of multi-objective optimization methods for engineering. *Struct. Multidiscip. Optim.* **2004**, *26*, 369–395. [CrossRef]

47. Flataker, A.F.; Sperstad, I.B.; Rana, R.; Korpås, M. How Important Is Fast-Charging Station Modelling in Distribution Grid Planning? Global Sensitivity Analysis of Grid Investment Model Output. *Sustain. Energy Grids Netw.* **2025**, *43*, 101721. [CrossRef]
48. Porru, M.; Serpi, A.; Mureddu, M.; Damiano, A. A Multistage Design Procedure for Planning and Implementing Public Charging Infrastructures for Electric Vehicles. *Sustainability* **2020**, *12*, 2889. [CrossRef]

Disclaimer/Publisher's Note: The statements, opinions and data contained in all publications are solely those of the individual author(s) and contributor(s) and not of MDPI and/or the editor(s). MDPI and/or the editor(s) disclaim responsibility for any injury to people or property resulting from any ideas, methods, instructions or products referred to in the content.